Washington University School of Medicine
Digital Commons@Becker

Open Access Publications

2021

Atoh7-independent specification of retinal ganglion cell identity

Justin Brodie-Kommit

Brian S Clark

Fion Shiau

Philip A Ruzycki

et al

Follow this and additional works at: https://digitalcommons.wustl.edu/open_access_pubs

NEUROSCIENCE

Atoh7-independent specification of retinal ganglion cell identity

Justin Brodie-Kommit[1]*, Brian S. Clark[2,3]*, Qing Shi[4†], Fion Shiau[2], Dong Won Kim[5], Jennifer Langel[6], Catherine Sheely[1], Philip A Ruzycki[2], Michel Fries[7,8], Awais Javed[7,8], Michel Cayouette[7,8,9,10], Tiffany Schmidt[11], Tudor Badea[12,13], Tom Glaser[14], Haiqing Zhao[1], Joshua Singer[4], Seth Blackshaw[5,15,16,17‡], Samer Hattar[6‡]

Copyright © 2021 The Authors, some rights reserved; exclusive licensee American Association for the Advancement of Science. No claim to original U.S. Government Works. Distributed under a Creative Commons Attribution NonCommercial License 4.0 (CC BY-NC).

Retinal ganglion cells (RGCs) relay visual information from the eye to the brain. RGCs are the first cell type generated during retinal neurogenesis. Loss of function of the transcription factor Atoh7, expressed in multipotent early neurogenic retinal progenitors leads to a selective and essentially complete loss of RGCs. Therefore, Atoh7 is considered essential for conferring competence on progenitors to generate RGCs. Despite the importance of Atoh7 in RGC specification, we find that inhibiting apoptosis in Atoh7-deficient mice by loss of function of Bax only modestly reduces RGC numbers. Single-cell RNA sequencing of Atoh7;Bax-deficient retinas shows that RGC differentiation is delayed but that the gene expression profile of RGC precursors is grossly normal. Atoh7;Bax-deficient RGCs eventually mature, fire action potentials, and incorporate into retinal circuitry but exhibit severe axonal guidance defects. This study reveals an essential role for Atoh7 in RGC survival and demonstrates Atoh7-dependent and Atoh7-independent mechanisms for RGC specification.

INTRODUCTION

The retina has six major classes of neurons that develop from a common progenitor cell pool during overlapping temporal intervals. Retinal ganglion cells (RGCs), the only projection neurons from the retina to the brain, are the first retinal cell type to be generated. RGC development in zebrafish, mice, and humans has been shown to require the basic helix-loop-helix transcription factor atonal homolog 7, Atoh7 (Math5) (1–8). Atoh7 is conserved across all vertebrate species and distantly related to atonal, which specifies the earliest-born neurons in Drosophila retina (1, 3, 7, 9). Atoh7-deficient mice and zebrafish lack upward of 95% of RGCs (1, 8, 10, 11) and likewise lack any visible optic nerve or functional connections from the retina to the brain (12, 13). Human mutations in ATOH7 or its cis-regulatory regions have been associated with optic nerve agenesis or hypoplasia (4, 6, 14) and increased susceptibility to glaucoma (15, 16). Atoh7 deficiency also disrupts the development of retinal vasculature in both mice and humans, likely as an indirect result of the loss of RGCs (17, 18).

In mice, Atoh7 is expressed in neurogenic retinal progenitor cells (RPCs) between E12 and P0, corresponding to the interval in which RGCs are generated (8, 19–26). Upon cell fate specification, Atoh7 expression is rapidly down-regulated in mouse RGC precursors (23, 27) although expression persists in immature human RGCs (28, 29). Genetic fate mapping indicates that Atoh7-expressing RPCs also give rise to other early-born retinal cells, including cone photoreceptors, horizontal, and amacrine cells, and that generation of these cell types is increased in Atoh7-deficient mice (1, 8, 12, 30). Although it has been reported that ectopic expression of Atoh7 can promote RGC formation in some situations (22, 31), it is typically not sufficient to drive RGC specification (22, 30, 32–38). However, misexpression of Atoh7 in Crx-expressing photoreceptor precursors was sufficient to rescue the development of a limited number of RGCs (22).

These findings have suggested that Atoh7 acts in neurogenic RPCs to confer competence to generate RGCs (10, 39, 40) potentially in combination with as yet unidentified factors. Recent experiments have shown that when Pou4f2 and Isl1 are expressed under the control of the endogenous Atoh7 promoter, these transcription factors are sufficient to fully rescue the defects in RGC development seen in Atoh7 mutants (32, 34, 37). This implies that Atoh7 may act permissively to enable the expression of these two factors in early-stage RPCs in order to generate RGCs.

Other data, however, suggest that a large number of RGCs are specified independently of Atoh7. Previous studies indicate that

[1]Department of Biology, Johns Hopkins University, Baltimore, MD, USA. [2]John F. Hardesty, MD, Department of Ophthalmology and Visual Sciences, Washington University School of Medicine, St. Louis, MO, USA. [3]Department of Developmental Biology, Washington University School of Medicine, St. Louis, MO, USA. [4]Department of Biology, University of Maryland, College Park, MD, USA. [5]Department of Neuroscience, Johns Hopkins University School of Medicine, Baltimore, MD, USA. [6]National Institute of Mental Health (NIMH), National Institutes of Health (NIH), Bethesda, MD, USA. [7]Cellular Neurobiology Research Unit, Institut de Recherches Cliniques de Montréal, Montréal, QC H2W 1R7, Canada. [8]Molecular Biology Programs, Université de Montréal, QC H3C 3J7, Canada. [9]Department of Anatomy and Cell Biology, McGill University, Montréal, QC H3A 0G4, Canada. [10]Department of Medicine, Université de Montréal, Montréal, QC H3T 1J4, Canada. [11]Department of Neurobiology, Northwestern University, Evanston, IL, USA. [12]National Eye Institute, National Institutes of Health,

Downloaded from http://advances.sciencemag.org/ on April 8, 2021

95% of RGCs in Atoh7 mutant retinas may suggest that Atoh7-independent RGCs require trophic support from either Atoh7-expressing RPCs or Atoh7-derived RGCs.

To distinguish the role of Atoh7 in controlling RGC specification and survival, we prevented RGC death in Atoh7-deficient mice by simultaneously inactivating the proapoptotic gene Bax (42, 43). The idea being if RGCs can be specified in the absence of Atoh7 but require it for trophic support, we should reveal RGCs that are specified in an Atoh7-independent manner when cell death is prevented. Notably, we observed only a 25.2 ± 0.9% reduction in adult RGC numbers in Atoh7$^{-/-}$;Bax$^{-/-}$ retinas relative to Bax$^{-/-}$ controls, implicating an unrecognized Atoh7-independent specification pathway for RGCs. While mutant RGCs showed severe defects in the formation of axonal projections and retinal vasculature, we found that the Atoh7-independent RGCs expressed both Pou4f2 and Isl1, the two transcription factors that are sufficient to fully compensate for Atoh7 function. These RGCs also fired action potentials in response to light and formed functional synapses with upstream retinal neurons. Single-cell RNA sequencing (scRNA-Seq) analysis of Atoh7;Bax-deficient retinas shows that Atoh7-deficient RGC differentiation is delayed relative to wild type (WT), implicating Atoh7 as responsible for generating early-born pioneering RGCs. Last, Cut&Run analysis indicates that Atoh7 directly activates genes enriched in RGC precursors while directly repressing genes enriched in neurogenic RPCs and photoreceptor precursors. Our results both identify a pathway for specifying RGCs that is independent of Atoh7 and clarify the mechanism of Atoh7 function during early retinal neurogenesis.

RESULTS

Atoh7 promotes RGC survival, but RGC specification is largely Atoh7 independent

In the absence of Atoh7, there is an increase in apoptosis of both Atoh7-derived cells across embryonic retinal development and non–Atoh7-derived cells in the ganglion cell layer (GCL) at embryonic day 16.5 (E16.5) and E17.5 (22, 25). These data suggest that Atoh7 may promote RGC survival in both a cell-autonomous and a non–cell-autonomous manner. To better understand the role that Atoh7 plays in RGC development, independent of its role in RGC survival, we disrupted both Atoh7 and the proapoptotic Bax gene in order to inhibit apoptosis in the retina.

We used Atoh7$^{Cre/Cre}$ mice, in which the Atoh7 coding sequence is replaced with Cre recombinase via targeted recombination, generating a null allele, to analyze Atoh7 function (40). We first examined the expression of RBPMS and Isl1, both of which are broadly expressed in RGCs, in Atoh7$^{Cre/Cre}$;Bax$^{-/-}$ mice (hereafter referred to as Atoh7$^{-/-}$;Bax$^{-/-}$ mice) (Fig. 1, A to C). Isl1, a LIM family homeodomain transcription factor, is necessary for RGC development and maintenance in adulthood (32, 44) and is expressed in mature

Specific RGC markers, Brn3a (Pou4f1) and Brn3b (Pou4f2), were used to quantify RGCs. For WT and Bax$^{-/-}$ lines, Brn3a and Brn3b numbers were similar to published reports (Fig. 1, D to F) (8, 22, 48, 49). In the Atoh7$^{-/-}$ line, a 99.8 ± 0.2% reduction in Brn3a RGC density was observed. However, in Atoh7$^{-/-}$;Bax$^{-/-}$ mice, the Brn3a RGCs were substantially rescued in the Atoh7$^{-/-}$ background and remained into adulthood. Brn3a RGCs (74.7 ± 6.9%) are rescued in Atoh7$^{-/-}$;Bax$^{-/-}$ mice relative to Bax$^{-/-}$ levels in adult, and RGCs display normal distribution across the entire retina (Fig. 1, D and E, fig. S1, A and A′; and fig. S2). Brn3b RGCs were also rescued in Atoh7$^{-/-}$;Bax$^{-/-}$ relative to Bax$^{-/-}$ retinas, but to a much lesser extent than the Brn3a (28.8 ± 3.9%; Fig. 1, D and F, and fig. S1, B and B′). Expression of Isl1, Brn3b, and, to a lesser extent, Brn3a has previously been reported to require Atoh7 (32, 37, 39, 44, 48, 50). However, our data demonstrate that the expression of Isl1, Brn3a, and Brn3b in RGCs can occur independent of Atoh7 (Fig. 1).

To investigate the extent to which rescued RGCs resembled WT neurons, we examined the expression of markers of major classes of mature RGCs. We investigated the prevalence of intrinsically photosensitive RGCs (ipRGCs) within Atoh7$^{-/-}$;Bax$^{-/-}$ retinas. During the development of ipRGCs, most cells express Brn3b, although, in some cases, only transiently (51). To determine the percentage of rescued ipRGCs in Atoh7$^{-/-}$;Bax$^{-/-}$ mice, we used a melanopsin antibody that predominantly labels the high melanopsin-expressing M1 and M2 ipRGC populations. We observe that 34.1% of ipRGCs are rescued in Atoh7$^{-/-}$;Bax$^{-/-}$ mice relative to Bax$^{-/-}$, proportions similar to the fraction of Brn3b-positive RGCs in WT (Fig. 1, D and F, and fig. S1, C to F). This indicates that rescued Brn3b-positive ipRGCs can differentiate in the absence of Atoh7.

To eliminate the possibility that global loss of function of Bax caused a nonspecific rescue of RGC development, we tested the effects of retina-specific conditional mutants of Bax, using Chx10-Cre; Atoh7$^{Cre/Cre}$;Bax$^{fl/fl}$ (Fig. 1, G and H). In this model, Bax is selectively disrupted in RPCs beginning at E10 to 10.5 (52). Removal of Bax from all RPCs shows RGC development to the same extent as in Atoh7$^{Cre/Cre}$;Bax$^{-/-}$ (Fig. 1, G and H). This indicates that the rescue of RGCs is specific to the retina.

We then reasoned that if cell death has to be rescued specifically in Atoh7-independent RGCs, then the number of RGCs should not be restored in Atoh7$^{Cre/Cre}$;Bax$^{fl/fl}$ mice. We observed that Atoh7$^{Cre/Cre}$; Bax$^{fl/fl}$ mice did not show any notable rescue of RGC numbers (Fig. 1, G and H), suggesting that preventing cell death in cells that do not express Atoh7 is sufficient for RGCs to differentiate and form connections with retinal neurons.

In both WT and Atoh7$^{-/-}$;Bax$^{-/-}$ animals, we observe that 34 ± 1.1% and 34 ± 1.6% of RGCs, respectively, are derived from Atoh7-expressing cells, a finding that independently confirms similar lineage tracings in previous studies (fig. S3, A to C) (10, 28). This indicates that while RGCs that are normally derived from Atoh7-expressing neurogenic RPCs are reduced in the absence of Atoh7, Atoh7 is not required for

Downloaded from http://advances.sciencemag.org/ on April 8, 2021

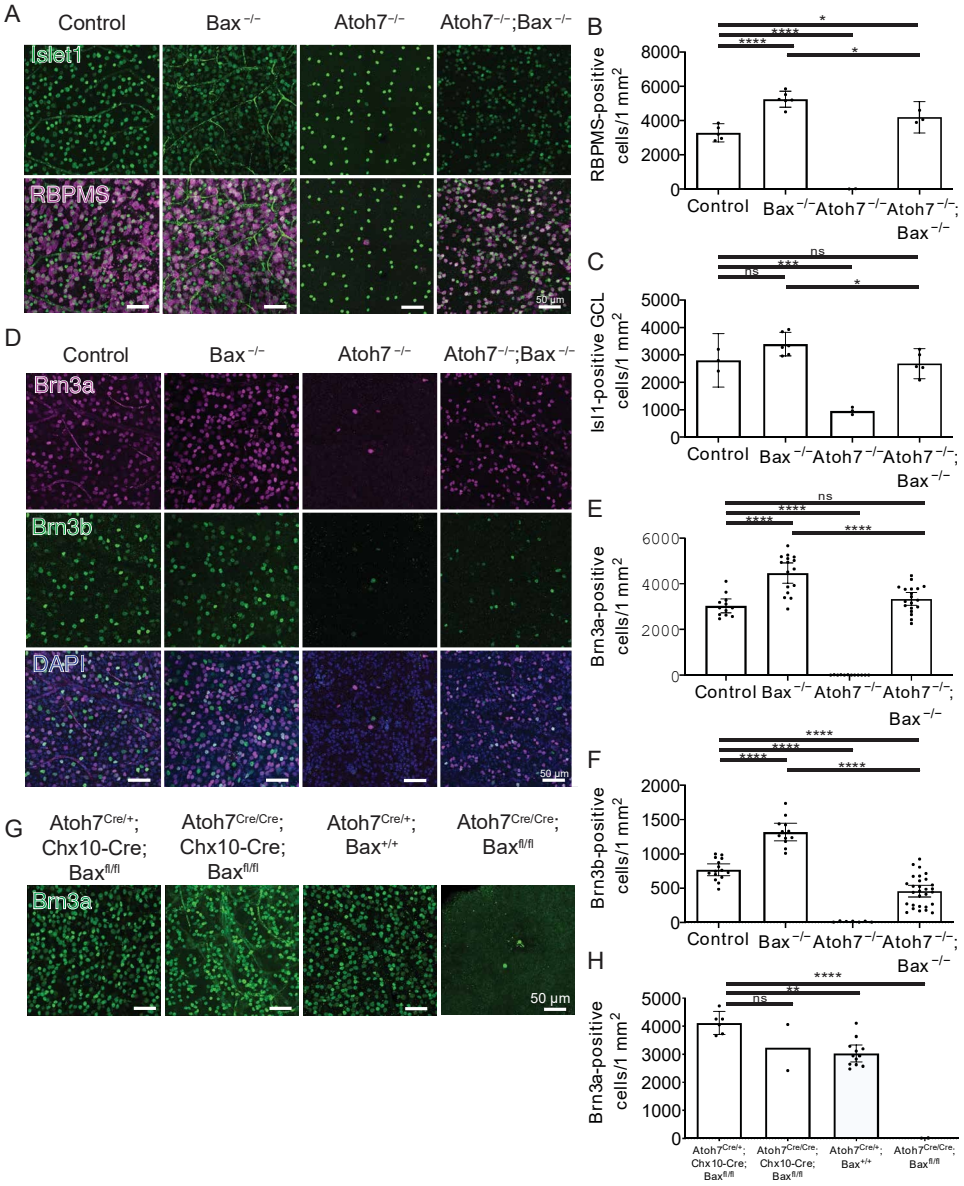

Fig. 1. Atoh7-independent development of RGCs. (A to C) We observed a 25.2 ± 0.9 and 21 ± 3% reduction in RBPMS$^+$ RGC density or Isl1$^+$ GCL cells when comparing Atoh7$^{-/-}$;Bax$^{-/-}$ to Bax$^{-/-}$ mice. (D to H) Brn3a and Brn3b positive RGC density are only moderately reduced when apoptosis is blocked in Atoh7$^{-/-}$;Bax$^{-/-}$ mice. (G and H) Brn3a positive RGC numbers are rescued when apoptosis is blocked in all neural RPCs, when Bax$^{lox/lox}$ is crossed to the Chx10-Cre transgene, which is expressed in all RPCs. However, when Bax is specifically removed in Atoh7-Cre knock in mice, Brn3a RGCs are not rescued. Means ± 95% confidence intervals. Statistical significance tested by one way analysis of variance (ANOVA) with Tukey's posttest for multiple comparisons *P < 0.045, **P = 0.0023, ***P < 0.0003, ****P < 0.0001. ns, non significant.

significant decrease in horizontal cells in the Atoh7$^{-/-}$;Bax$^{-/-}$ compared with Atoh7$^{-/-}$ but neither with control nor with Bax$^{-/-}$ (fig. S4, C and E). We observed a notable decrease in amacrine cells in

substantially increased by the loss of function of Atoh7 in the Bax mutant background.

Downloaded from http://advances.sciencemag.org/ on April 8, 2021

models. Spatiotemporal noise stimuli were used to activate the retina with a mean excitation of 398 nm (I_{mean} ≈ 3 × 10^3 photons cm^{-2} s^{-1}), a wavelength that predominantly activates S-cones (53) and does not activate Opn4-expressing ipRGCs (54–57). We observed an identical stimulus-response profile in WT and $Bax^{-/-}$ RGCs (Fig. 2A), an expected result given that $Bax^{-/-}$ mice display normal visual responses within the Morris water maze test (42). The population of RGCs included cells with similar light-evoked responses to ON sustained, ON transient, ON/OFF transient, OFF transient, or OFF sustained RGCs (Fig. 2A and fig. S5). The spatial receptive fields of the $Atoh7^{-/-}$;$Bax^{-/-}$ RGCs were slightly smaller than normal [$Atoh7^{-/-}$;$Bax^{-/-}$ average, 191 ± 7.1 μm (n = 96 from eight mice); control average, 212 ± 2.3 μm (n = 92 from five mice); and $Bax^{-/-}$ average, 223 ± 2.4 μm (n = 96 from four mice)] (Fig. 2B), and the kinetics of the light-driven responses in the $Atoh7^{-/-}$;$Bax^{-/-}$ retinas were slightly slower than those of control and $Bax^{-/-}$ cells (Fig. 2C).

The linear analysis used for the MEA data can only reveal an averaged spike-triggered averaging (STA), which could be a compression of multiple receptive fields. Thus, those having multiple receptive fields such as ON-OFF cells could potentially be hidden with this method and require more sophisticated analysis strategy (58). However, diversity in peristimulus time histogram (PSTH) profiles is clearly observed, suggesting that different cell types coexist in $Atoh7^{-/-}$;$Bax^{-/-}$ mice. We chose not to perform more complex analysis such as classifying each cell into known cell types due to the relatively small sample size. These will be intriguing questions to address when larger amounts of data are made accessible. The near-normal properties of the $Atoh7^{-/-}$;$Bax^{-/-}$ RGCs show that RGCs present in the $Atoh7^{-/-}$;$Bax^{-/-}$ are wired properly to the outer retina, specifically the S-cones, and receive normal circuit input.

RGC axon guidance is Atoh7 dependent

While RGCs in $Atoh7^{-/-}$;$Bax^{-/-}$ animals appropriately respond to the detection of visual stimuli by the outer retina, the ability of these RGCs to form postsynaptic connections in the brain is compromised. We observed a substantially reduced pupillary light response (PLR) in $Atoh7^{-/-}$;$Bax^{-/-}$ animals compared to controls (Fig. 3, B and C). To determine the cause of behavioral deficits, we assessed the distribution of RGC axons. Immunostaining for Smi32 (nonphosphorylated Nfh) (Fig. 3, A and D, and fig. S6C), Nfh, and Nfm (fig. S6, A and B) was used to evaluate RGC axonal integrity and showed normal architecture in WT and $Bax^{-/-}$ mice. We were surprised to find that the <1% of RGCs that survive in the $Atoh7^{-/-}$ showed severe guidance defects. These RGCs fasciculate, come in close proximity to where the optic disc should be, seem to overshoot the optic disc, and then continue to extend within the retina. The great majority of $Atoh7^{-/-}$ RGC axons fail to correctly target the optic disc, with only a few axons exiting and forming a rudimentary optic nerve, leading to a severely reduced PLR (Fig. 3, B and C, and fig. S7, A to C). The gross misguidance of axons was also observed in $Atoh7^{-/-}$;$Bax^{-/-}$ mice

in large numbers. These findings are reminiscent of previous reports in zebrafish, in which morpholino-mediated disruption of atoh7 expression in early-stage RPCs disrupted the correct targeting of axons of later-born, atoh7-positive RGCs to the optic tectum (33).

Previous studies have observed a lack or massive reduction in physical or functional connection to the brain in $Atoh7^{-/-}$ mice (1, 12, 13, 59). Consistent with the failure of mutant RGCs to correctly target the optic nerve, we observe severe disruptions in behavioral responses to light in $Atoh7^{-/-}$;$Bax^{-/-}$ mice that are essentially indistinguishable from those seen in $Atoh7^{-/-}$ mice. $Atoh7^{-/-}$;$Bax^{-/-}$ mice show no detectable optokinetic response (fig. S9A) and show no visual cue–dependent reduction in escape time during successive trials of the Morris water maze (fig. S9B). Opn4:Tau-lacZ knock-in mice, which visualize the axonal projections of M1 ipRGCs, show no detectable signal in the brain in $Atoh7^{-/-}$;$Bax^{-/-}$ (fig. S9C) (55). Intraocular injection of fluorescently labeled cholera toxin beta, which visualizes RGC axonal terminals (60), likewise shows no brain labeling in both $Atoh7^{-/-}$;$Bax^{-/-}$ and $Atoh7^{-/-}$ mice (fig. S9D). However, while the contralateral PLR is significantly reduced compared to WT in both the $Atoh7^{-/-}$ and $Atoh7^{-/-}$;$Bax^{-/-}$ mice, it is, nonetheless, detectable, indicating that a small number of RGC axons target the olivary pretectal nucleus in $Atoh7^{-/-}$;$Bax^{-/-}$ mice, although we are unable to detect these using standard techniques (Fig. 3, B and C, and fig. S7, A to C).

Retinal vasculature development is disrupted in the absence of Atoh7

In both mice and humans, loss of Atoh7 expression results in persistence of the hyaloid vasculature (2, 17, 61). The persistence of the hyaloid vasculature in $Atoh7^{-/-}$ retinas until P14 was previously observed. We likewise observe persistence of the hyaloid vasculature into adulthood in $Atoh7^{-/-}$ retinas (Fig. 4E). Unexpectedly, even with the rescue of a majority of Brn3a RGCs in $Atoh7^{-/-}$;$Bax^{-/-}$ animals, the hyaloid vasculature still fails to regress (Fig. 4E). Likewise, Crx>Atoh7;$Atoh7^{-/-}$ mice, in which Atoh7 is misexpressed in photoreceptor precursors, also fail to induce hyaloid regression (Fig. 4E). This is in sharp contrast to the rescued vascular phenotype observed in $Atoh7^{tTA/tTA}$;B&I-EE mice, when Brn3b and Isl1 are ectopically expressed from the endogenous Atoh7 locus in a Atoh7-deficient mouse using the tet-off system (Figure 4E) (37), and implies that Brn3b and Isl1 may activate the expression of secreted factors that drive vascular regression in a narrow time window during development.

scRNA-seq analysis of RGCs generated in the absence of Atoh7

To examine potential differences in RGC development within $Atoh7^{-/-}$ and $Atoh7^{-/-}$;$Bax^{-/-}$ compared to WT and $Bax^{-/-}$ control animals, we next performed scRNA-seq on $Bax^{-/-}$, $Atoh7^{-/-}$, and $Atoh7^{-/-}$;$Bax^{-/-}$ retinas to more comprehensively profile changes in cell-type speci-

Downloaded from http://advances.sciencemag.org/ on April 8, 2021

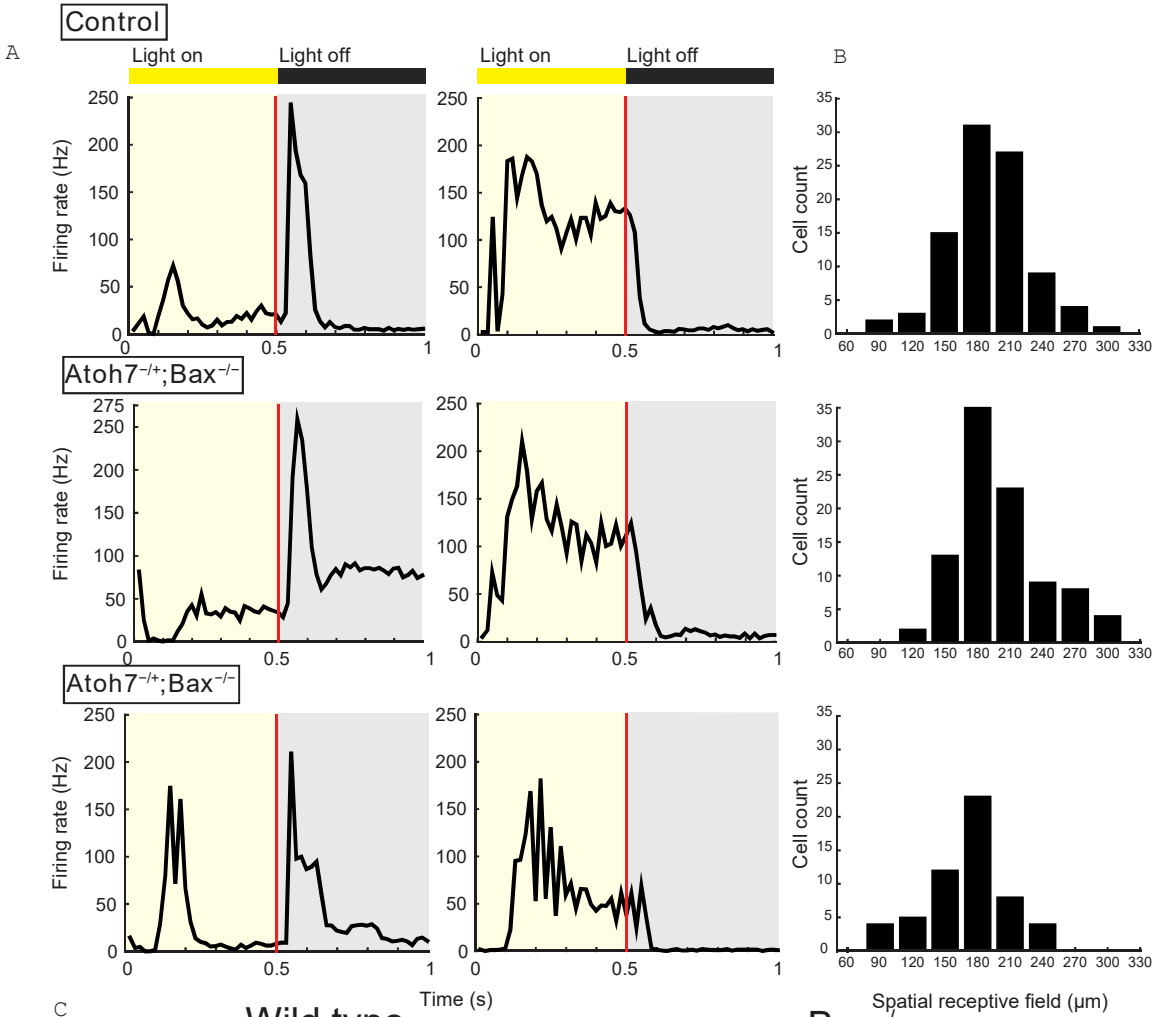

Downloaded from http://advances.sciencemag.org/ on April 8, 2021

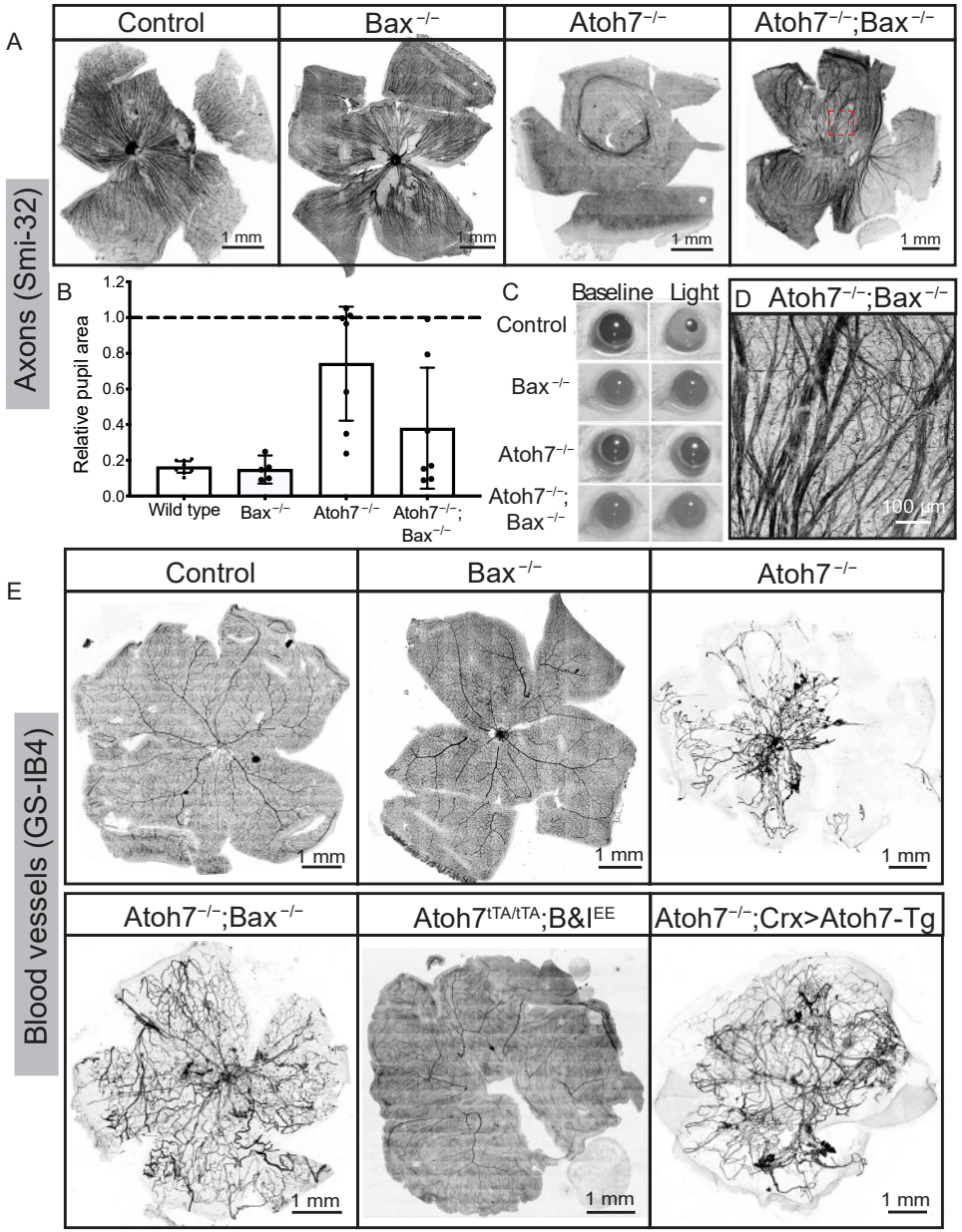

Fig. 3. RGC axon guidance and retinal vasculature development require Atoh7-dependent RGCs. (A and D) Smi-32 labels a subset of RGCs and their axons in an adult WT retina. In Atoh7$^{-/-}$ mice, the Smi-32–positive RGCs have axon guidance deficits. In Atoh7$^{-/-}$;Bax$^{-/-}$ mice, RGCs have severe axon guidance deficits. Highlighted region (A, Atoh7$^{-/-}$;Bax$^{-/-}$) is magnified in (D). (B and C) Using the contralateral PLR as a readout of retina to brain connection allows the appreciation that the severe axon guidance deficits allow for some connection to the brain of the RGCs in the Atoh7$^{-/-}$ or Atoh7$^{-/-}$;Bax$^{-/-}$ retinas. (E) It has been previously reported that the hyaloid vasculature fails to regress in Atoh7$^{-/-}$ mice, thought to be due to lack of RGCs; however, when the RGC numbers are rescued, in Atoh7$^{-/-}$;Bax$^{-/-}$ mice, the hyaloid vasculature fails to regress. However, Atoh7 is not necessary for the hyaloid regression and retinal vasculature development, seen using Atoh7$^{tTA/tTA}$;B&I^{EE} mice, which was previously seen to rescue all of the Atoh7 null phenotypes. When Atoh7 is rescued using the Crx>Atoh7 transgene on the Atoh7 null background, the optic nerve and 12% of RGCs are rescued (22), but the hyaloid vasculature does not regress.

Downloaded from http://advances.sciencemag.org/ on April 8, 2021

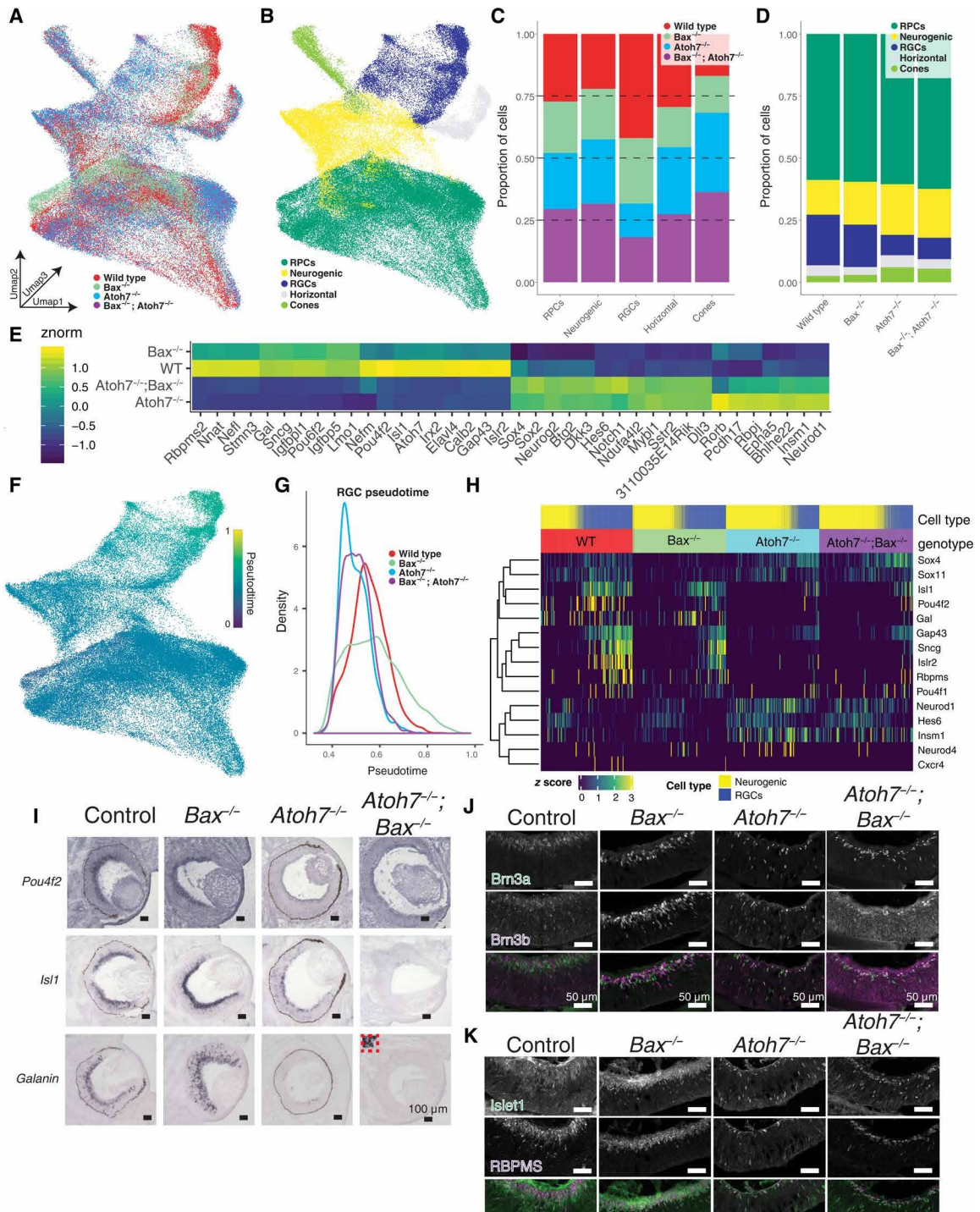

Downloaded from http://advances.sciencemag.org/ on April 8, 2021

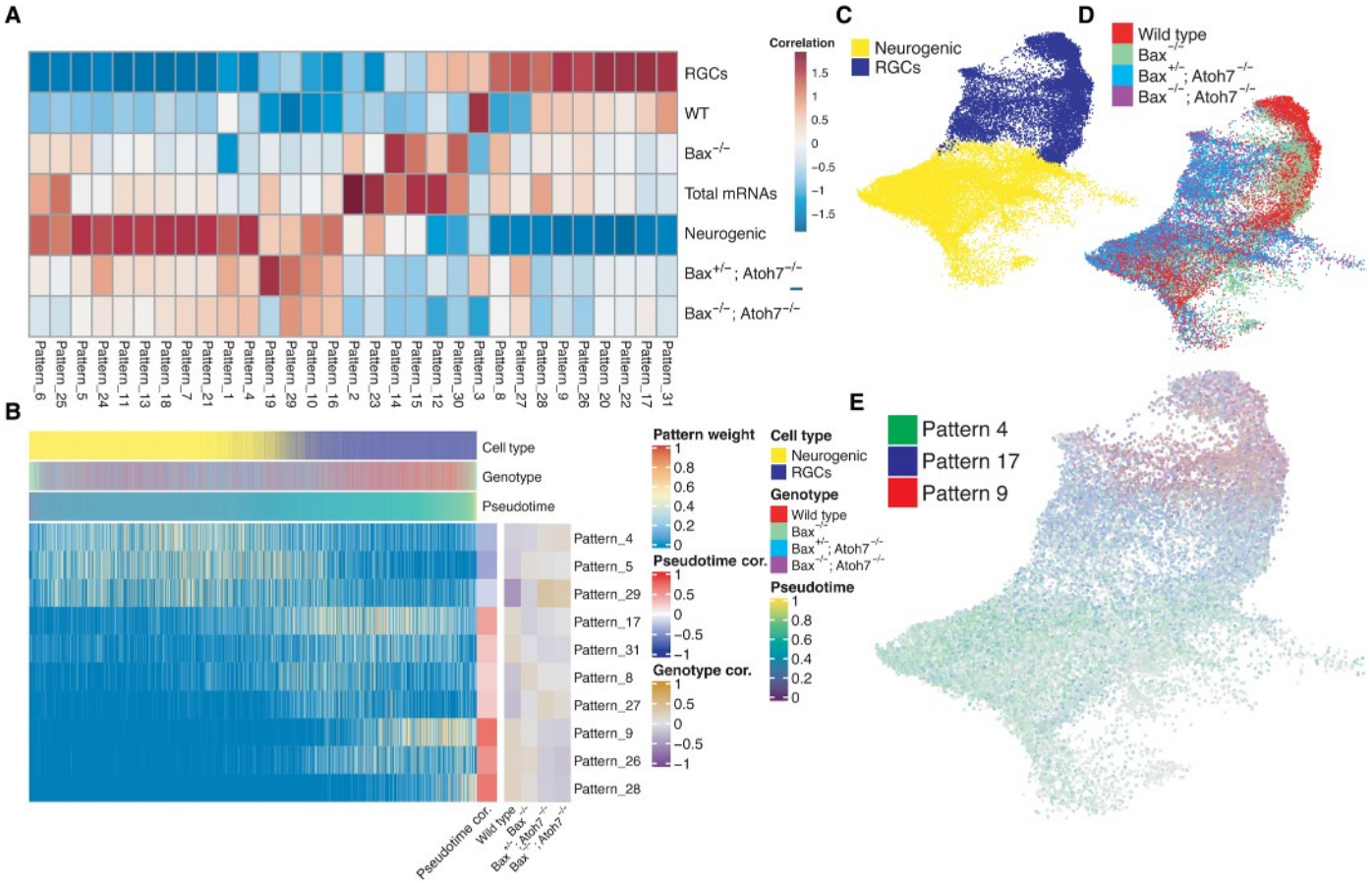

Fig. 5. scCoGAPS analysis of single-cell dataset and RGC population changes in E12.5 retinas show a developmental delay in Atoh7$^{-/-}$;Bax$^{-/-}$ mutants. (A) Heat map showing the correlation between scCoGAPS pattern and cellular features. (B) Heatmap of pattern weights within individual cells ordered by pseudotime. Pattern correlations with both pseudotime and each genotype are displayed on the right. (C to E) UMAP embedding of single cell dataset used for scCoGAPS and colored by (C) cell type or (D) genotype. (E) UMAP embedding of dataset and colored by pattern weights of scCoGAPS patterns 4, 17, and 9, displaying progressive pattern usage across RGC development.

Pou4f2 (Brn3b), Isl1, Pou6f2 (Rpf-1), Elavl4, Gap43, and Irx2 (fig. S11B) (64–67). Conversely, differentially expressed transcripts enriched in the Atoh7 knockout samples (Fig. 4E) were enriched for genes involved in the Notch signaling pathway—Rbpj, Dll3, Notch1, and Hes6—and for transcripts enriched in neurogenic cells and photoreceptor precursors during retinal development—Btg2, Neurog2, Bhlhe22, Insm1, Neurod1, Mybl1, Sstr2, and 3110035E14Rik (fig. S11B) (23).

Atoh7-deficient RGCs also show dramatically reduced expression of genes known to regulate axon guidance, including the cell adhesion molecule Islr2, which has been found to control RGC axon fasciculation, as well as axon guidance at the optic chiasm (68). Of particular interest are the observed increases in Rbpj and with a recovery in the specification of RGC numbers in adult Atoh7$^{-/-}$;Bax$^{-/-}$ animals, these data suggest that loss of Atoh7 expression leads to an increase in expression of genes specific to neurogenic RPCs at the expense of RGC-enriched transcripts; results are consistent with a developmental delay.

As albino mice are known to have fewer ipsilaterally projecting RGCs (71) and because Bax$^{-/-}$ mice are on an albino background, we specifically examined the expression of transcripts traditionally down-regulated in albino mice. Most of these transcripts are down-regulated in Bax$^{-/-}$ retinas at E14.5; however, these ipsilateral transcripts were similar to WT in both Atoh7$^{-/-}$ and Atoh7$^{-/-}$;Bax$^{-/-}$ E14.5 retinas (fig. S11C) (71), suggesting that the albino background does

Downloaded from http://advances.sciencemag.org/ on April 8, 2021

results are consistent with a failure of maturation or developmental delay of RGC specification in Atoh7-deficient RGCs (Fig. 4G). Differential expression analysis assessing for differences between the genotypes' pseudotemporal gene expression dynamics revealed significant genotypic differences across RGC development (Fig. 4H and table S2).

In both Atoh7$^{-/-}$ and Atoh7$^{-/-}$;Bax$^{-/-}$ samples, we observed a reduction of expression in many genes enriched within mature RGCs—Pou4f2, Gap43, Sncg, and Isl1. We likewise observed reduced expression of a subset of genes in neurogenic RPCs, including Gal. Increased expression of other genes predominantly expressed in neurogenic RPCs, including Neurod1, Insm1, Neurod4, Hes6, Onecut1, Onecut2, and Sox4, is observed in both Atoh7-deficient neurogenic RPCs and RGCs compared to controls (Fig. 4H). This implies that loss of function of Atoh7 may delay the differentiation of RGCs from neurogenic RPCs. The temporal expression patterns of genes involved in RGC specification mimic those observed within additional E14 scRNA-seq datasets (62), and analyses of transcriptomic changes resulting from loss of Atoh7 expression closely match those obtained from scRNA-seq–based analysis of Atoh7$^{-/-}$ retina conducted at E13.5 (73).

We next performed in situ hybridization to examine changes in global transcript expression within the developing retina. RNA transcript expression was detected at E14.5, at which point most RGCs are specified (19, 20), and we observed decreased expression of Pou4f2 (Brn3b), Isl1, and Gal in both Atoh7$^{-/-}$ and Atoh7$^{-/-}$;Bax$^{-/-}$ mice, as determined by chromogenic in situ hybridization (Fig. 4I). Immunostaining of E14 retinas confirms a reduction in the number of cells immunopositive for Brn3a (Pou4f1) and Brn3b (Pou4f2) (Fig. 4J), as well as the pan-RGC markers RBPMS and Isl1 (Fig. 4K), in the developing GCL of Atoh7-deficient retinas. At E12.5, we observed a marked decrease in both overall RGC density and RGC number (fig. S8). Together, these results suggest that loss of function of Atoh7 delays RGC differentiation and leads to an accumulation of neurogenic RPCs.

To further identify patterns of temporal changes in gene expression across RGC genesis between Atoh7 mutant and control retinas, we performed the nonnegative matrix factorization analysis of the Bayesian NMF technique Single Cell Coordinated Gene Activity in Pattern Sets (scCoGAPS) (74). Implementation of scCoGAPS parses the gene expression into groups ("patterns") based on gene expression profiles without a priori, literature-based knowledge of gene interactions. Using 5235 highly variable genes across the 29,182 neurogenic RPCs and differentiating RGCs, we identified 31 patterns of gene expression (Fig. 5, A, B, and E, and fig. S12). These patterns correlated with both neurogenic RPC—patterns 6, 25, 5, 24, 11, 13, 18, 7, 21, 1, and 4—and RGC—patterns 8, 27, 28, 9, 26, 20, 22, 17, and 31—cell-type annotations and highlighted temporal changes in gene expression, as assessed through pseudotime analyses (Fig. 5, A, B, and E). Individual patterns, patterns 4, 5, and 29, with control samples (Fig. 5, A, B, and E). The most highly weighted genes in patterns 9 and 26 are Gap43 and Igfbpl1, respectively, which have been implicated in RGC axonal growth (75, 76). Pattern 28 highlights cells toward the end of the RGC trajectory and is largely driven by Sncg, a transcript enriched in most RGCs in the adult mouse retina (Fig. 5, A and B) (77). The association of neurogenic patterns with Atoh7$^{-/-}$ mutant retinas versus those that highlight RGC differentiation and maturation patterns with control retinas further support a developmental delay in mutant RGCs. Analysis of pattern marker expression across the genotypes (fig. S12) highlights both the temporal delay and global changes in gene expression across the Atoh7$^{-/-}$ mutant retinas compared to controls.

Recent studies have comprehensively profiled RGC subtype diversity in the mouse retina (78, 79). However, these studies did not characterize either the birthdates of individual RGC subtypes or the transcriptional networks controlling RGC subtype specification. The delay in RGC maturation and the failure of optic nerve formation seen in Atoh7-deficient retinas suggest that the earliest pathfinding RGCs are Atoh7 dependent. We examined expression of markers of mature RGC subtypes (78) within the developing retina and correlated expression of the transcripts with RGC pseudotime (fig. S13), as many of the mature RGC subtype markers are not specific to RGCs. We detected expression of selective markers for a fraction of mature RGC subtypes within the E14.5 scRNA-seq dataset. Of transcripts in which readily detectable expression was observed, many—including Igfbp4, Foxp1, Stxbp6, Bhlhe22, and Penk—also display enriched expression in primary or neurogenic RPCs. Expression of some markers of RGC development and maturation—Ebf3, Pou4f1, Pou4f2, Prdm8, and Slc17a6—correlated well with pseudotemporal ordering and were depleted in Atoh7-deficient RGCs. However, a limited number of RGC subtype markers, including Irx3, Calb2, and Tac1, were largely absent from Atoh7 mutant RGCs.

Atoh7 binds to loci associated with neurogenic RPC, RGC, and photoreceptor-enriched genes

To gain insight into the function of Atoh7 during RGC specification, we performed Cut&Run experiments (80) on E14 mouse retinas using the established Atoh7 antibody (27) and immunoglobulin G (IgG) as a control. Peak calling was performed using the MACS2 pipeline (81). High concordance of called peaks is observed between Atoh7 Cut&Run replicates (fig. S14A), with >3000 shared peaks and little enrichment of peak sequences within the IgG sample. Comparisons of Atoh7 peaks to developmental chromatin accessibility (82) determined that peaks proximal to gene transcription start sites, corresponding to proximal promoters, exhibited high accessibility throughout retinal development (fig. S14B). Distal peaks, corresponding to enhancer sequences (>3 kb from the transcription start sites), however, displayed the greatest accessibility during early periods of retinal development when RGCs are being

Downloaded from http://advances.sciencemag.org/ on April 8, 2021

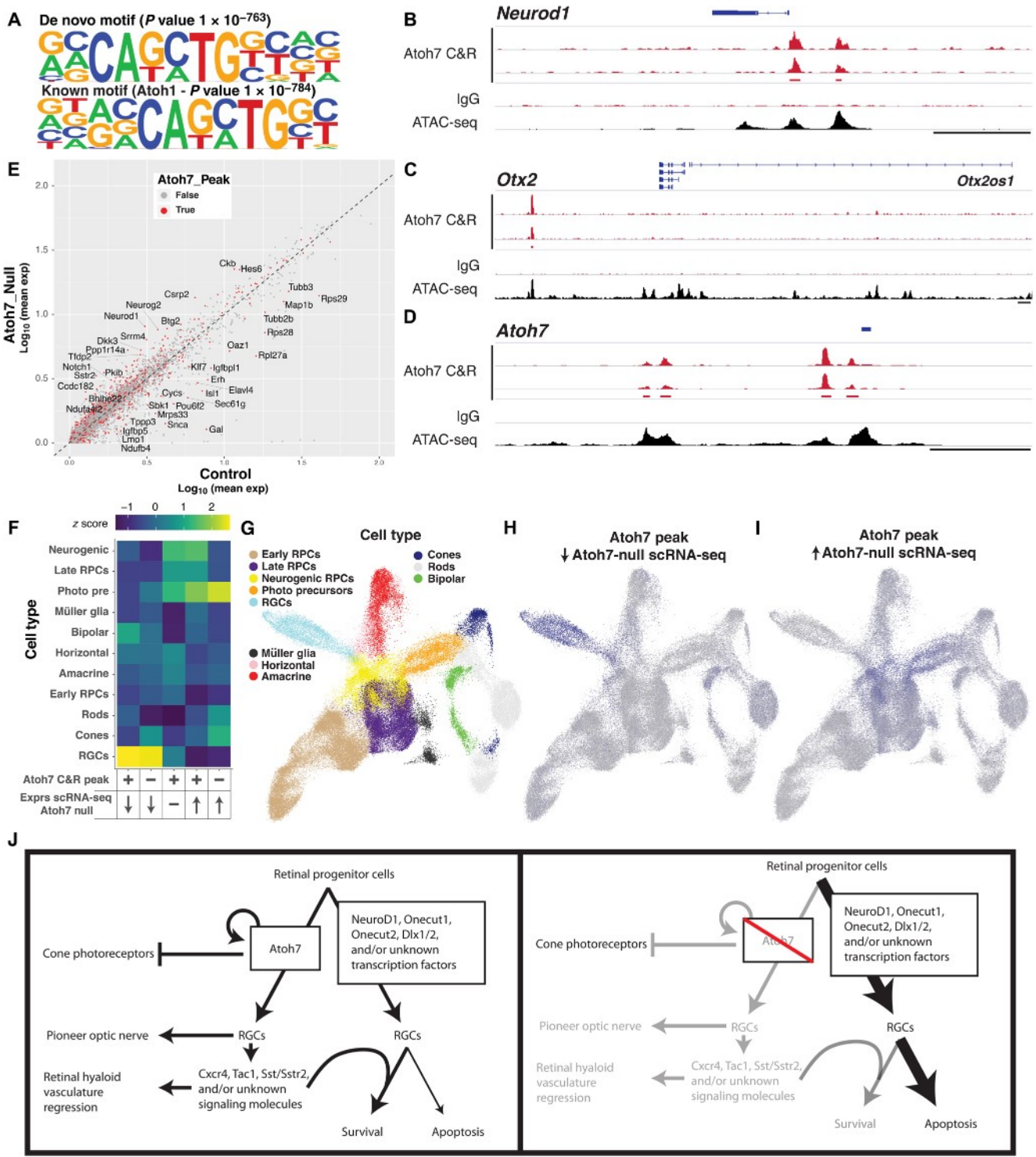

Downloaded from http://advances.sciencemag.org/ on April 8, 2021

We next assigned peaks to genes using ChIPSeeker (84). Many strong peaks were located within genetic loci of transcripts with known functions during early retinal development, including Neurod1, Elavl4, Neurog2, Pou6f2, Otx2, Meis2, and Lhx4 (Fig. 6, B to E, and table S5). We also observed strong enrichment of Atoh7 binding within the Atoh7 proximal promoter and distal enhancer sequences (14), suggestive of autoregulation of Atoh7 expression (Fig. 6D). In addition, we detected Atoh7 binding within numerous loci associated with RGCs, including Rbpms, Pou4f2, Isl1, and Pou4f1 (fig. S14, C to F, and table S5); however, the binding sites of Atoh7 within the Pou4f2 locus are located within the intron of the neighboring gene Ttc29 and, therefore, are assigned to Ttc29 instead of Pou4f2.

To better understand the mechanism by which Atoh7 regulates transcription of nearby genes, we next examined the consequence of Atoh7 loss of function on bound loci gene expression, as determined by our scRNA-seq experiments in control (WT and $Bax^{-/-}$) versus Atoh7 null ($Atoh7^{-/-}$ and $Atoh7^{-/-}$;$Bax^{-/-}$) neurogenic cells and RGCs (fig. S15). Our analyses indicated that many Atoh7-bound genes display decreased expression within Atoh7 mutant retinas, including the RGC-enriched genes Pou6f2, Elavl4, Isl1, and Tubb2b (Fig. 6E). Conversely, roughly similar numbers of "bound" genes displayed increased expression in Atoh7 mutant retinas, including neurogenic RPC-enriched transcripts Hes6, Btg2, Neurod1, Neurog2, Sstr2, Pkib, and Bhlhe22 (Fig. 6E) (23). To gain further insight into the biological relevance of Atoh7-bound and differentially expressed transcripts, we first binned transcripts into five categories: (i) Atoh7-bound and down-regulated in Atoh7 mutants, (ii) Atoh7-bound and up-regulated in Atoh7 mutants, (iii) no binding and down-regulated in Atoh7 mutants, (iv) no binding and up-regulated in Atoh7 mutants, and (v) Atoh7-bound but no change in expression. Following binning, we calculated the z scores of gene expression on an individual cell basis using the mouse retinal development single-cell dataset (23) and examined the enrichment of expression of binned genes within annotated cell types. Our analysis determined that Atoh7-bound genes that displayed decreased expression in Atoh7 mutant retinas show enriched expression in RGCs, suggesting an active role of Atoh7 in promoting RGC fate (Fig. 6, F to H). Conversely, Atoh7-bound genes that are up-regulated in Atoh7 mutant retinas display high expression within neurogenic cells or photoreceptor precursors and include Neurod1, Neurog2, and Hes6 (Fig. 6, F and I). We also observe Atoh7 binding within additional cone photoreceptor gene loci, including Lhx4, Otx2, and Thrb (table S5), although these genes did not display robust differences in gene expression between control and Atoh7 mutant retinas. The up-regulation of Atoh7-bound neurogenic and photoreceptor-enriched genes in Atoh7 mutant retinas suggest that Atoh7 actively represses photoreceptor fate during early retinogenesis, an interpretation that is supported by the observed modest increase in cone photoreceptor proportions within Atoh7 mutant scRNA-seq samples (Fig. 4D).

Galanin is not the Atoh7-dependent secreted factor that

clear Atoh7-dependent expression in our scRNA-seq dataset. The neuropeptide galanin (Gal), which is strongly expressed in both neurogenic RPCs and RGCs and is a direct target of Atoh7 (Fig. 6E), was by far the most differentially expressed secreted factor in Atoh7-deficient mice (Fig. 4, E and F, and Fig. 6E; and table S1). Galanin has been implicated in promoting the survival of neural precursors (85, 86) and to be enriched in ipsilaterally projecting RGCs (62). However, Gal-deficient animals showed no differences in either the hyaloid vasculature regression or RGC density, as compared to the control animals (fig. S16).

DISCUSSION

It is broadly accepted that Atoh7 acts in RPCs as a competence factor that is essential for RGC specification (10, 39, 40, 87). In this study, though, we show that the specification of the great majority of RGCs occurs even in the absence of Atoh7. While RGC specification can occur independent of Atoh7, Atoh7 function is required to maintain RGC survival and proper targeting of RGC axons to the optic nerve head (Fig. 6J). Following disruption of both Atoh7 and Bax, we observe only a 20% reduction in the number of RGCs relative to Bax-deficient controls. This compares to a greater than 95% reduction in RGC numbers in Atoh7 mutants relative to WT controls. Although RGCs in $Atoh7^{-/-}$;$Bax^{-/-}$ retinas show severe defects in targeting the optic nerve head, they respond robustly to photoreceptor stimulation.

The presence of functional RGCs in the absence of Atoh7 helps explain long-standing, puzzling observations: (i) 45% of RGCs are not derived from Atoh7-expressing progenitors, (ii) molecular markers of RGCs are observed at considerably higher levels during early stages of retinal development than in adults in Atoh7-deficient retinas, and (iii) the marked increase in apoptosis in the GCL that occurs in the absence of Atoh7 (10, 32, 35). Previous studies have implicated Atoh7 as a direct upstream regulator of the essential RGC transcription factors Brn3a, Brn3b, and Isl1. Supporting this, an Atoh7 hierarchy of RGC determinants, studies in which Brn3b and Isl1 were inserted in place of the Atoh7 coding sequence observed a complete rescue of normal RGC development (37). Our studies, however, indicate that when apoptosis is inhibited, Brn3a, Brn3b, Islet1, and Rbpms expression is induced at near-normal levels within RGCs in both E14 and adult retinas, independent of Atoh7 expression. We observe that Atoh7 binds to sites in the Isl1 and Pou4f1 (Brn3a) loci (fig. S14, E and F), suggesting active regulation of Isl1 and Brn3a transcription by Atoh7. While no Atoh7 Cut&Run peak was assigned to Pou4f2 (Brn3b), two Atoh7-binding sites were identified in the terminal intron of Pou4f2-neighboring gene Ttc29 (fig. S14D). While further evidence is required to clearly demonstrate that Atoh7 regulates Pou4f2 expression via these binding sites, we observed reduced expression of Isl1, Pou4f1, and Pou4f2 within Atoh7-deficient retinal cells. Therefore, we conclude that other factor(s) in addition to Atoh7 activate expression of these genes.

Downloaded from http://advances.sciencemag.org/ on April 8, 2021

as we did not observe RGC rescue within Atoh7$^{Cre/Cre}$;Bax$^{fl/fl}$ mice, we suggest that immature RGCs rapidly degenerate as the result of the lack of an Atoh7-dependent survival factor. This wave of developmental apoptosis has been observed previously, but the underlying molecular mechanisms are unknown (46, 47, 88–92). We hypothesize that this prosurvival factor or factors must be produced by either Atoh7-expressing neurogenic RPCs or RGCs derived from these cells.

Our data also reveal a marked delay in the formation of RGCs from neurogenic RPCs in the absence of Atoh7. This is consistent with previous results in Atoh7$^{-/-}$ retinas, where RGC formation is delayed by at least a day, in part due to RPCs remaining in cell cycle (22, 93). However, this delay in cell cycle exit later resolves, as essentially normal levels of all other early-born cell types in the Atoh7$^{-/-}$;Bax$^{-/-}$ retinas, including RGCs (Fig. 1 and fig. 4). When Atoh7-dependent RGCs are rescued later in development, as seen in targeted mutants in which Atoh7 is expressed from the endogenous Crx locus, the hyaloid vasculature regression was not rescued, even though a modest rescue of RGC formation is observed (22). Consistent with this result, loss of function of atoh7 in early-stage RPCs in the zebrafish retina disrupts the correct targeting of axons in later-born RGCs to the optic nerve (33). Together with the fact that 45% of RGCs arise from a non–Atoh7-dependent lineage in mice, we hypothesize that early, pathfinding RGCs are Atoh7 dependent and provide both survival and guidance cues for later-born RGCs.

Since Atoh7 was previously thought to be a master transcriptional regulator of RGC specification, strategies aimed at targeted differentiation of RGCs for therapeutic purposes have focused on using the forced expression of Atoh7. We, however, now appreciate RGC specification to be a far more complicated process. Although ectopic expression of Atoh7 activates expression of RGC-specific genes in cultured RPCs (94), induced pluripotent stem cells (95), and Müller glia-derived retinal stem cells (96, 97), it is, nonetheless, typically not sufficient to drive these cells to become RGCs. This study sheds light on why this may be the case.

These findings demonstrate that additional factors act in parallel to Atoh7 to control RGC specification. While multiple other transcription factors have been reported to regulate RGC specification, including Neurod1, Sox4, and Onecut2 (35, 98, 99), these factors are unable to individually activate expression of Brn3b and Isl1. In Atoh7$^{-/-}$;Bax$^{-/-}$ RGCs, however, we observe substantially increased expression of each of these transcription factors (Fig. 4E and fig. S12), suggesting the possibility that these factors, among others, may compensate for the loss of Atoh7. The observations that Atoh7 binds to target sites in the genomic loci of multiple genes that are up-regulated in Atoh7 mutant retinas, including Neurod1, Neurog2, Otx2, and Onecut2, suggest that Atoh7 directly inhibits alternate mechanisms of RGC genesis. However, the identity of the non–cell-autonomous cues by which Atoh7 regulates RGC survival, axon guidance, and hyaloid vasculature regression remains unknown (Fig. 6J). Further identification of the mechanisms regulating the in-

Use Committee) guidelines, and we used protocols approved by the Johns Hopkins University Animal Care and Use Committee (protocol number MO16A212). Atoh7$^{Cre/Cre}$ mice are a knock-in line where Cre recombinase replaced the entire Atoh7 gene and was a gift from L. Gan (referred to as Atoh7$^{-/-}$) (RRID:MGI:3717726) (40). The Bax$^{tm1Sjk/tm1Sjk}$ (Bax$^{-/-}$) mice containing a neomycin cassette that replaces critical exons 2 to 5 were purchased from the Jackson Laboratory (JAX:002994, RRID:IMSR_JAX:002994) (43). The Bax$^{-/-}$ mice are unpigmented since the Bax gene is linked to the Tyrosinase (Tyr) and Pink-eyed dilution (p) gene by 21 and 5 cM, respectively. The conditional Bax$^{tm2Sjk/tm2Sjk}$ (Bax$^{fl/fl}$) mice containing LoxP sites flanking exons 2 to 4 were purchased from the Jackson Laboratory (JAX:006329, RRID:IMSR_JAX:006329) (100). Atoh7$^{tTA/tTA}$;B&I-EE mice are a combination of two genetic strains. In the first strain (Atoh7$^{tTA/tTA}$), the tetracycline-responsive artificial transcription factor tTA replaces the Atoh7 gene. In the absence of tetracycline, the tTA activates the tetracycline-responsive element that is driving the expression of Brn3b and Isl1 in the second strain (B&I-EE). Therefore, in effect, the Atoh7 promoter will drive the expression of Brn3b and Isl1. This mouse line has been previously reported to rescue all reported effects of Atoh7 loss of function and was a gift from X. Mu (MGI:5749708 and MGI:5749713) (37). The Crx>Atoh7 mice, a transgene that expresses the full-length Atoh7 coding sequence under the control of the Crx promoter, was previously published (MGI:5433215) (22). A tdTomato Cre recombinase reporter mouseRosa26^{tdTomAi14} (JAX:007914, RRID:IMSR_JAX:007914) (101) was used to label cells in a Cre recombinase–dependent manner. The Chx10-Cre mouse line is a transgenic line purchased from the Jackson Laboratory, originally developed by C. Cepko's laboratory (JAX:005105, RRID:IMSR_JAX:005105) (52), and expresses Cre recombinase broadly in all RPCs from E10 to E15.5. The Opn4^{taulacZ} mice were used to trace the ipRGC projections to the brain (55). Throughout the manuscript, controls are heterozygous for both Atoh7 and Bax (Atoh7$^{+/-}$;Bax$^{+/-}$), whereas Atoh7$^{-/-}$ mice were also heterozygous for Bax (Atoh7$^{-/-}$;Bax$^{+/-}$).

Statistics

All statistical tests, apart from analysis of the scRNA-seq data, were performed in GraphPad Prism 6 (RRID:SCR_002798). The statistical tests used are listed in figure captions.

Immunohistochemistry

Adult retinas from P40 to P200 mice were obtained by enucleating whole eyes, fixing for 30 min in 4% paraformaldehyde (PFA) diluted in phosphate-buffered saline (PBS), dissecting to remove the cornea and lens, and dissecting the retina from the RPE, and antibody staining proceeded in a 24-multiwell cell culture plate (Corning, no. 353047). Retinas were blocked in 500 μl of PBS containing 0.3% Triton X-100 and 6% goat serum for 2 hours at room temperature (RT). Several antibodies were used in this study (dilutions are in

Downloaded from http://advances.sciencemag.org/ on April 8, 2021

no. C9205, RRID:AB_476889) (1:1000), GS-IB4 (Molecular Probes, catalog nos. I21411 and I21411, RRID:AB_2314662) (1:250), Rabbit anti-Pax2 (BioLegend, catalog no. 901001, RRID:AB_2565001) (1:100), Mouse anti-Tuj1 (R&D Systems, catalog no. MAB1195, RRID:AB_357520) (1:200), Rabbit anti-DsRed (Takara Bio, catalog no. 632496, RRID:AB_10013483) (1:250), Mouse anti-Islet1 (DSHB, catalog no. 40.2D6, RRID:AB_528315) (1:200), and Rabbit anti-Opn4 (Advanced Targeting Systems, catalog no. UF006, RRID:AB_2314781) (1:500), Rabbit anti-Pax6 (Millipore, catalog no. AB2237, RRID:) (1:500), Mouse anti-Rxrgamma (Santa Cruz Biotechnology, catalog no. sc-365252, RRID:AB_10850062) (1:200), Rabbit anti-Cone arrestin (Millipore, catalog no. AB15282, RRID:AB_1163387) (1:1000), and Mouse anti-calbindin (Sigma-Aldrich, catalog no. C9848, RRID:AB_476894) (1:1000). The appropriate antibodies were diluted in blocking solution and incubated for 2 days at 4°C. Retinas were then washed in three changes of PBS, 15 min in each, and then placed in the appropriate Alexa Fluor secondary antibody (1:500; Invitrogen) overnight at 4°C. Retinas were washed in 200 of PBS containing 1× DAPI (4′,6-diamidino-2-phenylindole), then washed three times in PBS for 15 min each, and mounted flat on slides in VectaShield (Vector Labs, RRID:AB_2336789). Regionalized dissections were done as follows: Before enucleation, the most nasal part of the sclera was marked with a cauterizer. This mark was used during the dissection to make a marking incision into the retina, following the above staining protocol. Retinas were imaged on a Zeiss LSM 700 or 800 confocal microscope at the Johns Hopkins University Integrated Imaging Center Core Facility (RRID:SCR_016187).

For embryonic studies, developing embryos harvested at E12.5 and E14.5 were washed in a petri dish with sterile PBS three times for 10 min. Tail was used for genotyping. The heads were fixed in 4% PFA for 30 min and then cryoprotected in 30% sucrose at 4°C overnight, frozen in optimal cutting temperature compound (OCT), and sectioned at 18- thickness using a cryostat. Sections were dried at 30°C for 15 min and then washed for 10 min in three changes of PBS. Sections were then blocked and stained as above in a humidified chamber overnight. Sections were then mounted and imaged as described.

Cell density analysis

All cell counting was done manually. To confirm the reproducibility of the cell counts, randomly selected selections from each sample were counted twice, and counts were consistently found to be essentially identical. Density was calculated as the number of cells per area. All measurements and cell number analysis were done manually in ImageJ (Fiji, RRID:SCR_002285) and Adobe Photoshop CS6 (RRID:SCR_014199).

In adult flat-mounted retinas, the density of RGCs was calculated by obtaining at least four representative images at 40× of 600 × 600 with 1- optical sections. Optical sections were projected together with maximum intensity, including cells only in the retinal layers of interest. Representative images were taken similarly across

chosen for analysis were all positive for $Pax2^+$ optic nerve head cells, as the central retina contains the earliest-born RGCs. At least two sections with matching criteria were analyzed for each E12.5 embryo. Density was calculated by dividing the number of $Brn3a^+$ RGCs and dividing by the area of the retina. To limit the analysis to the RGC neurogenic zone, we limited the quantification to the leading edge of RGC genesis. The percentage of mature $Brn3a^+$ RGCs at E12.5 was determined by counting their number within the GCL. The number of mature $Brn3a^+$ RGCs was then divided by the number of total $Brn3a^+$ RGCs in a section and then averaged across all sections. This ratio represents the number of $Brn3a^+$ RGCs already in the nascent GCL versus RGCs migrating through the neuroblast layer to the GCL.

MEA recordings

Mice were dark-adapted for 1 to 2 hours before being euthanized and dissected under dim red light. Retinas were isolated in Ames' medium (Sigma-Aldrich) bubbled with 95% O_2/5% CO_2 (carbogen) at RT, trimmed into small rectangles, and then placed on a 6 × 10 perforated MEA (Multichannel Systems, Tübingen, Germany), ganglion cell side down. Tissue was perfused with Ames' bubbled with carbogen and kept at 32°C throughout the experiment. Data acquisition was performed using the MC_Rack software (ALA Scientific Instruments Inc.), at a 50-kHz sampling rate. An offline spike sorter (Plexon Inc.) was used for spike sorting.

Ultraviolet stimuli (I_{mean} 10^3 photons cm^{-2} s^{-1}, 398 nm) were generated through a modified DLP projector (HP Notebook Projection Companion Projector, model HSTNN-FP01) (frame rate 60 Hz) and were delivered through an inverted microscope objective. All stimuli were programmed using the Psychophysics Toolbox in Matlab (MathWorks, Natick, MA). Stimuli include the following: (i) 120-s, 1-Hz full-field square-wave flash (100% Michelson contrast); (ii) 10-min Gaussian white noise (GWN) flickering checkerboard (pixel size 44.77); and (iii) 10-min spatially correlated "cloud" stimulus that was generated by low-pass filtering the GWN. The cloud stimulus introduced dark and bright areas of a range of scales within each frame, with the purpose of driving large spatial receptive fields.

The analysis was first performed using custom-written Matlab (MATLAB R2014b) codes; the results later were exported and edited in Adobe Illustrator CS6. For each cell, the PSTH of responses to square-wave flash was calculated using 10-ms bins. Spatial and temporal receptive fields were identified on the basis of noise data using a nonlinear model previously described in detail (58, 103).

Fewer cells were recorded from $Atoh7^{Cre/Cre}$;$Bax^{-/-}$ mice compared to the WT and $Bax^{-/-}$, as the nerve fiber layer (NFL) and retinal vasculature are improperly developed and, thus, provide an insulating layer that needs to be removed in order to obtain high-quality recordings. No cells were recorded from $Atoh7^{Cre/Cre}$ mice due to the >99% reduction in RGC numbers.

Downloaded from http://advances.sciencemag.org/ on April 8, 2021

contralateral or ipsilateral eye to the light source. The baseline pupil size of each mouse was first recorded for at least 5 s using an infrared light source, following which the white LED bulb was turned on for at least 30 s. Video recordings were analyzed by creating screenshot images in Joint Photographic Experts Group format (jpg) of the pupil before and during light stimulation using VLC media player (www.videolan.org/vlc/). The pupil area was then quantified in ImageJ (Fiji, RRID:SCR_002285). To determine the relative pupil area, pupil size during the light stimulation was divided by pupil size before light stimulation.

Tissue dissociation for generation of single-cell suspensions

Eyes were enucleated from E14 time-pregnant animals and placed directly into ice-cold 1× PBS. Retinas were dissected in cold 1× PBS and then placed into 200 μl of cold HBSS (Hanks' balanced salt solution) per two to three retinas. Tissue dissociation was induced through the addition of an equivalent volume of papain solution [1 ml to 700 μl of reagent grade water, 100 μl of fresh 50 mM L-cysteine (Sigma-Aldrich), 100 μl of 10 mM EDTA, and 10 μl of 60 mM 2-mercaptoethanol (Sigma-Aldrich), with papain added to 1 mg/ml (1:10 dilution of 10 mg/ml papain solution; Worthington)]. The papain-retina mixture was placed at 37°C for 10 min with slight trituration every 2 to 3 min. Enzymatic dissociation was halted through the addition of 600 μl of Neurobasal media and 10% FBS for every 400 μl of dissociation solution. DNA from lysed cells was removed using 5 μl of RNase-free DNase I (Roche) for every 1 ml of dissociated cells and incubated at 37°C for 5 min, followed by slight trituration using a 1-ml pipette. Cells were pelleted after centrifugation [300 RCF (relative centrifugal force) for 5 min at 4°C], followed by resuspension in 2 to 3 ml of Neurobasal media supplemented with 1% FBS. The final solution was passed through a 50-μm filter to remove cellular aggregates and undissociated debris.

10x Genomics sequencing and analysis

scRNA-seq of dissociated retinal cells from E14 Atoh7$^{-/+}$;Bax$^{-/-}$ and Atoh7$^{-/-}$;Bax$^{-/-}$ was performed using the 10x Genomics Chromium 3′ v2 platform (PN-120223) (Pleasanton, CA), followed by sequencing using the NextSeq 500 platform with default 10× sequencing parameters [R1, 26 base pairs (bp); R2, 98 bp; i7, 8 bp]. Single-cell analysis of the WT E14 developing mouse retina was obtained from previously reported samples obtained from GEO (GSE118614); data obtained using similar isolation protocols are described previously (23).

Gene set usage pattern discovery with scCoGAPS

CoGAPS v.3.5.6 (74, 104) was used to find patterns of gene set usage by neurogenic and retinal ganglion cells. The expression matrix used as input was normalized to 10,000 counts per cell, subsetted down to 5235 most highly variable genes, and $\log_2$-transformed. The CoGAPS parameters used are as follows: singleCell = TRUE,

differentialGeneTest(dat[genes expressed in >=10 cells], fullModelFormulaStr = '~(Atoh7 genotype) + Total_mRNAs', reducedModelFormulaStr = '~Total_mRNAs',cores=4).

Pseudotime analysis between genotypes

Scanpy v1.4 (72) was first used to assign diffusion pseudotime values (105) to cells in the RGC trajectory. Cell types included in this final dataset were restricted to RGCs, primary RPCs, and neurogenic RPCs. To preprocess the dataset, genes <10 counts were removed, and the expression matrix was normalized to 10,000 counts per cell and log-transformed. Highly variable genes used for ordering were identified using Scanpy's "highly_variable_genes" function with default parameters except flavor = "cell_ranger" and n_top_genes = 3000. Fifty principal components were calculated using default PCA (principal components analysis) parameters with random_state = 123,456. To compute the neighborhood graph with the batch effect of genotype removed, we used BBKNN with batch_key = "Genotype" and neighbors_within batch = 5 (106). Ten diffusion components were then computed and used for input to assign diffusion pseudotime values with an RPC cell as root. To find genes differentially expressed between the developmental trajectories of the WT and Atoh7$^{Cre/Cre}$; Bax$^{-/-}$ genotypes, Monocle's differential gene test (107, 108) was performed in R, on neurogenic RPCs and RGCs of WT and Atoh7$^{Cre/Cre}$; Bax$^{-/-}$ null genotypes:

differentialGeneTest(dat[genes expressed in >=10 cells], fullModelFormulaStr = '~sm.ns(Pseudotime,df=3)*Genotype+ Total_mRNAs', reducedModelFormulaStr = '~sm.ns(Pseudotime, df=3)+Genotype+Total_mRNAs',cores=3).

In situ hybridization

Developing embryos harvested at E14.5 were washed in petri dishes filled with sterile DEPC (diethyl pyrocarbonate)–treated PBS at least three times. The head of the embryo was plunged into OCT and then immediately frozen and stored at −80°C until needed, and the tail was used for genotyping. Sections (20 μm) were taken using a cryostat. Sections were allowed to dry on slides for a few hours and then were stored at −80°C until needed. In situ hybridization was performed as previously described (109).

Cut&Run

Five retinas from E14 C57BL6/J embryos were dissected and pooled per biological replicate and processed for Cut&Run as described in (80) with a few modifications. All steps were carried out in 0.2 ml of PCR (polymerase chain reaction) tube strips and 22 μl of BioMag Concanavalin A beads (Polysciences, catalog no. 86057-3) suspended in an additional 100 μl per sample of binding buffer [20 mM Hepes (pH 7.9), 10 mM KCl, 1 mM $CaCl_2$, and 1 mM $MnCl_2$]. After two washes, the beads were resuspended in 10 μl per sample of binding buffer using a magnetic rack. Retinas were dissociated by pipetting and centrifuged for 3 min at 300g in PBS at RT. Cells were then re-

Downloaded from http://advances.sciencemag.org/ on April 8, 2021

antibodies were added to the samples and incubated at 4°C overnight. Supernatant was cleared the next day, and the cell/bead mix was gently resuspended in 200 µl of cold buffer 3 (buffer 1 and 0.01% digitonin). After two washes, cell/bead mix was gently resuspended in 50 µl of cold buffer 3. One microliter of 50× pAG-MNase was added to the cell/bead mix and incubated at RT for 10 min. Cold buffer 3 (200 µl) was added to wash the cell/bead mix twice. Supernatant was discarded, and the cell/bead mix was resuspended in 50 µl of cold buffer 3. $CaCl_2$ (100 mM) was added, and the samples were incubated on ice for 30 min. Thirty-three microliters of stop buffer [340 mM NaCl, 20 mM EDTA, 4 mM EGTA, RNase A (50 µg/ml), and glycogen (50 µg/ml)] was added to the cell/bead mix, and the samples were incubated for 10 min at 37°C. Beads were discarded, and the supernatant was used to extract DNA using the Qiagen nucleotide removal kit as per the manufacturer's specifications. DNA was eluted in 20 µl of elution buffer and sent for library preparation. Libraries were prepared per the manufacturer's instructions using the KAPA HyperPrep Kit (Roche) and sequenced using the Illumina HiSeq 4000 sequencing system with 2 × 50 bp of sequencing parameters.

Cut&Run data processing

Paired-end reads were aligned to mm10 with Bowtie2 v2.3.5 under parameters "--local --very-sensitive-local --no-unal --no-mixed--no-discordant --phred33 -I 10 -X 700," as described previously (110, 111). Samtools filtered out alignments with less than a 30 MAPQ score (112). Picard v2.0.1 MarkDuplicates removed duplicate reads. MACS2 v2.2.7.1 called peaks with the following parameters: "-t Atoh7_bed -c IgG_bed -f BED -g mm --keep-dup all -p 1e-5 -n output_file" (81). bedtools found an overlap between the two replicates' peaks with "intersect -u -a Rep1.narrowPeak -b Rep2.narrowPeak" (113). Overlapping peaks aligning to mitochondrial or random chromosomes were removed. Homer v4.11 was used for motif discovery by using "findMotifsGenome.pl" under default parameters (83). In ChIPseeker v1.22.1, "annotatePeak" was used to annotate the overlapping peaks with genomic features (84). DeepTools v3.1.0 was used to generate bigwig files for visualization (default parameters and bin size of 5 bp) and for coverage heatmaps (114).

SUPPLEMENTARY MATERIALS

Supplementary material for this article is available at http://advances.sciencemag.org/cgi/content/full/7/11/eabe4983/DC1

View/request a protocol for this paper from Bio-protocol.

REFERENCES AND NOTES

1. N. L. Brown, S. Patel, J. Brzezinski, T. Glaser, Math5 is required for retinal ganglion cell and optic nerve formation. Development 128, 2497–2508 (2001).
2. N. M. Ghiasvand, D. D. Rudolph, M. Mashayekhi, J. A. Brzezinski IV, D. Goldman, T. Glaser, Deletion of a remote enhancer near ATOH7 disrupts retinal neurogenesis, causing NCRNA disease. Nat. Neurosci. 14, 578–586 (2011).
3. A. P. Jobling, F. H. Grell, L. Ackerman, L. Y. Jan, Y. N. Jan, Atonal is the proneural gene for Drosophila photoreceptors and is expressed in the disc ectoderm during eye development. Proc. Natl. Acad. Sci. U.S.A. 95, 8853–8858 (1998).
4. E. S. Tai, T. Y. Wong, C. M. van Duijn, T. Aung, Genome-wide association studies in Asians confirm the involvement of ATOH7 and TGFBR3, and further identify CARD10 as a novel locus influencing optic disc area. Hum. Mol. Genet. 20, 1864–1872 (2011).
6. S. Macgregor, A. W. Hewitt, P. G. Hysi, J. B. Ruddle, S. E. Medland, A. K. Henders, S. D. Gordon, T. Andrew, B. M. Evoy, P. G. Sanfilippo, F. Carbonaro, V. Tah, Y. J. Li, S. L. Bennett, J. E. Craig, G. W. Montgomery, K. N. Tran Viet, N. L. Brown, T. D. Spector, N. G. Martin, T. L. Young, C. J. Hammond, D. A. Mackey, Genome-wide association identifies ATOH7 as a major gene determining human optic disc size. Hum. Mol. Genet. 19, 2716–2724 (2010).
7. L. Prasov, T. Masud, S. Khaliq, S. Q. Mehdi, A. Abid, E. R. Oliver, E. D. Silva, A. Lewanda, M. C. Brodsky, M. Borchert, D. Kelberman, J. C. Sowden, M. T. Dattani, T. Glaser, ATOH7 mutations cause autosomal recessive persistent hyperplasia of the primary vitreous. Hum. Mol. Genet. 21, 3681–3694 (2012).
8. S. W. Wang, B. S. Kim, K. Ding, H. Wang, D. Sun, R. L. Johnson, W. H. Klein, L. Gan, Requirement for math5 in the development of retinal ganglion cells. Gene Dev. 15, 24–29 (2001).
9. S. Kanekar, M. Perron, R. Dorsky, W. A. Harris, L. Y. Jan, Y. N. Jan, M. L. Vetter, Xath5 participates in a network of bHLH genes in the developing Xenopus retina. Neuron 19, 981–994 (1997).
10. J. A. Brzezinski IV, L. Prasov, T. Glaser, Math5 defines the ganglion cell competence state in a subpopulation of retinal progenitor cells exiting the cell cycle. Dev. Biol. 365, 395–413 (2012).
11. J. N. Kay, K. C. Finger Baier, T. Roeser, W. Staub, H. Baier, Retinal ganglion cell genesis requires lakritz, a zebrafish atonal homolog. Neuron 30, 725–736 (2001).
12. J. A. Brzezinski IV, N. L. Brown, A. Tanikawa, R. A. Bush, P. A. Sieving, M. H. Vitaterna, J. S. Takahashi, T. Glaser, Loss of circadian photoentrainment and abnormal retinal electrophysiology in Math5 mutant mice. Invest. Opthalmol. Vis. Sci. 46, 2540–2551 (2005).
13. R. Wee, A. M. Castrucci, I. Provencio, L. Gan, R. N. V. Gelder, Loss of photic entrainment and altered free-running circadian rhythms in math5$^{-/-}$ mice. J. Neurosci. 22, 10427–10433 (2002).
14. J. B. Miesfeld, N. M. Ghiasvand, B. Marsh Armstrong, N. Marsh Armstrong, E. B. Miller, P. Zhang, S. K. Manna, R. J. Zawadzki, N. L. Brown, T. Glaser, The Atoh7 remote enhancer provides transcriptional robustness during retinal ganglion cell development. Proc. Natl. Acad. Sci. U.S.A. 117, 21690–21700 (2020).
15. W. D. Ramdas, L. M. E. van Koolwijk, H. G. Lemij, F. Pasutto, A. J. Cree, G. Thorleifsson, S. F. Janssen, T. B. Jacoline, N. Amin, F. Rivadeneira, R. C. W. Wolfs, G. B. Walters, F. Jonasson, N. Weisschuh, C. Y. Mardin, J. Gibson, R. H. C. Zegers, A. Hofman, P. T. V. M. de Jong, A. G. Uitterlinden, B. A. Oostra, U. Thorsteinsdottir, E. Gramer, U. C. Welgen Bussen, J. F. Kirwan, A. A. B. Bergen, A. Reis, K. Stefansson, A. J. Lotery, J. R. Vingerling, N. M. Jansonius, C. C. W. Klaver, C. M. van Duijn, Common genetic variants associated with open angle glaucoma. Hum. Mol. Genet. 20, 2464–2471 (2011).
16. B. J. Fan, D. Y. Wang, L. R. Pasquale, J. L. Haines, J. L. Wiggs, Genetic variants associated with optic nerve vertical cup-to-disc ratio are risk factors for primary open angle glaucoma in a US caucasian population. Invest. Opthalmol. Vis. Sci. 52, 1788–1792 (2011).
17. M. M. Edwards, D. S. McLeod, R. Li, R. Grebe, I. Bhutto, X. Mu, G. A. Lutty, The deletion of Math5 disrupts retinal blood vessel and glial development in mice. Exp. Eye Res. 96, 147–156 (2012).
18. M. L. O'Sullivan, V. M. Puñal, P. C. Kerstein, J. A. Brzezinski IV, T. Glaser, K. M. Wright, J. N. Kay, Astrocytes follow ganglion cell axons to establish an angiogenic template during retinal development. Glia 65, 1697–1716 (2017).
19. R. W. Young, Cell differentiation in the retina of the mouse. Anat. Rec. 212, 199–205 (1985).
20. R. L. Sidman, Histogenesis of mouse retina studied with Thymidine H 3, in Anatomica Record (DIV JOHN WILEY & SONS INC., New York, 1960) vol. 136, pp. 276–277.
21. N. L. Brown, S. Kanekar, M. L. Vetter, P. K. Tucker, D. L. Gemza, T. Glaser, Math5 encodes a murine basic helix-loop-helix transcription factor expressed during early stages of retinal neurogenesis. Development 125, 4821–4833 (1998).
22. L. Prasov, T. Glaser, Pushing the envelope of retinal ganglion cell genesis: Context

Downloaded from http://advances.sciencemag.org/ on April 8, 2021

26. M. Pacal, R. Bremner, Induction of the ganglion cell differentiation program in human retinal progenitors before cell cycle exit: Kinetics of ganglion cell differentiation. Dev. Dynam. 243, 712–729 (2014).
27. J. B. Miesfeld, T. Glaser, N. L. Brown, The dynamics of native Atoh7 protein expression during mouse retinal histogenesis, revealed with a new antibody. Gene Exp. Patterns 27, 114–121 (2018).
28. Y. Lu, F. Shiau, W. Yi, S. Lu, Q. Wu, J. D. Pearson, A. Kallman, S. Zhong, T. Hoang, Z. Zuo, F. Zhao, M. Zhang, N. Tsai, Y. Zhuo, S. He, J. Zhang, G. L. Stein O'Brien, T. D. Sherman, X. Duan, E. J. Fertig, L. A. Goff, D. J. Zack, J. T. Handa, T. Xue, R. Bremner, S. Blackshaw, X. Wang, B. S. Clark, Single-cell analysis of human retina identifies evolutionarily conserved and species-specific mechanisms controlling development. Dev. Cell 53, 473–491.e9 (2020).
29. J. G. Aparicio, H. Hopp, A. Choi, J. M. Comar, V. C. Liao, N. Harutyunyan, T. C. Lee, Temporal expression of CD184(CXCR4) and CD171(L1CAM) identifies distinct early developmental stages of human retinal ganglion cells in embryonic stem cell derived retina. Exp. Eye Res. 154, 177–189 (2017).
30. R. B. Hufnagel, A. N. Riesenberg, M. Quinn, J. A. Brzezinski, T. Glaser, N. L. Brown, Heterochronic misexpression of Ascl1 in the Atoh7 retinal cell lineage blocks cell cycle exit. Mol. Cell. Neurosci. 54, 108–120 (2013).
31. X. M. Zhang, T. Hashimoto, R. Tang, X. J. Yang, Elevated expression of human bHLH factor ATOH7 accelerates cell cycle progression of progenitors and enhances production of avian retinal ganglion cells. Sci. Rep. 8, 6823 (2018).
32. L. Pan, M. Deng, X. Xie, L. Gan, ISL1 and BRN3B co-regulate the differentiation of murine retinal ganglion cells. Development 135, 1981–1990 (2008).
33. A. J. Pittman, M. Y. Law, C. B. Chien, Pathfinding in a large vertebrate axon tract: Isotypic interactions guide retinotectal axons at multiple choice points. Development 135, 2865–2871 (2008).
34. L. Gan, S. W. Wang, Z. Huang, W. H. Klein, POU domain factor Brn-3b is essential for retinal ganglion cell differentiation and survival but not for initial cell fate specification. Dev. Biol. 210, 469–480 (1999).
35. C. A. Mao, J. H. Cho, J. Wang, Z. Gao, P. Pan, W. W. Tsai, X. Mu, L. J. Frishman, W. H. Klein, Reprogramming amacrine and photoreceptor progenitors into retinal ganglion cells by replaceing Neurod1 with Atoh7. Development 140, 2849–2849 (2013).
36. C. A. Mao, S. W. Wang, P. Pan, W. H. Klein, Rewiring the retinal ganglion cell gene regulatory network: Neurod1 promotes retinal ganglion cell fate in the absence of Math5. Development 135, 3379–3388 (2008).
37. F. Wu, T. J. Kaczynski, S. Sethuramanujam, R. Li, V. Jain, M. Slaughter, X. Mu, Two transcription factors, Pou4f2 and Isl1, are sufficient to specify the retinal ganglion cell fate. Proc. Natl. Acad. Sci. U.S.A. 112, E1559–E1568 (2015).
38. S. F. Ohnuma, S. Hopper, K. C. Wang, A. Philpott, W. A. Harris, Co-ordinating retinal histogenesis: Early cell cycle exit enhances early cell fate determination in the Xenopus retina. Development 129, 2435–2446 (2002).
39. X. Mu, X. Fu, H. Sun, P. D. Beremand, T. L. Thomas, W. H. Klein, A gene network downstream of transcription factor Math5 regulates retinal progenitor cell competence and ganglion cell fate. Dev. Biol. 280, 467–481 (2005).
40. Z. Yang, K. Ding, L. Pan, M. Deng, L. Gan, Math5 determines the competence state of retinal ganglion cell progenitors. Dev. Biol. 264, 240–254 (2003).
41. L. Poggi, M. Vitorino, I. Masai, W. A. Harris, Influences on neural lineage and mode of division in the zebrafish retina in vivo. J. Cell Biol. 171, 991–999 (2005).
42. S. K. Chen, K. S. Chew, D. S. McNeill, P. W. Keeley, J. L. Ecker, B. Q. Mao, J. Pahlberg, B. Kim, S. C. S. Lee, M. A. Fox, W. Guido, K. Y. Wong, A. P. Sampath, B. E. Reese, R. Kuruvilla, S. Hattar, Apoptosis regulates ipRGC spacing necessary for rods and cones to drive circadian photoentrainment. Neuron 77, 503–515 (2013).
43. C. M. Knudson, K. S. K. Tung, W. G. Tourtellotte, G. A. J. Brown, S. J. Korsmeyer, Bax-deficient mice with lymphoid hyperplasia and male germ cell death. Science 270, 96–99 (1995).
44. X. Mu, X. Fu, P. D. Beremand, T. L. Thomas, W. H. Klein, Gene regulation logic in retinal ganglion cell development: Isl1 defines a critical branch distinct from but overlapping with Pou4f2. Proc. Natl. Acad. Sci. U.S.A. 105, 6942–6947 (2008).
45. R. W. Young, Cell death during differentiation of the retina in the mouse. J. Comp. Neurol. 229, 362–373 (1984).
49. M. Xiang, L. Zhou, J. P. Macke, T. Yoshioka, S. H. Hendry, R. L. Eddy, T. B. Shows, J. Nathans, The Brn-3 family of POU-domain factors: Primary structure, binding specificity, and expression in subsets of retinal ganglion cells and somatosensory neurons. J. Neurosci. 15, 4762–4785 (1995).
50. X. Mu, P. D. Beremand, S. Zhao, R. Pershad, H. Sun, A. Scarpa, S. Liang, T. L. Thomas, W. H. Klein, Discrete gene sets depend on POU domain transcription factor Brn3b/Brn-3.2/POU4f2 for their expression in the mouse embryonic retina. Development 131, 1197–1210 (2004).
51. S. K. Chen, T. C. Badea, S. Hattar, Photoentrainment and pupillary light reflex are mediated by distinct populations of ipRGCs. Nature 476, 92–95 (2011).
52. S. Rowan, C. L. Cepko, Genetic analysis of the homeodomain transcription factor Chx10 in the retina using a novel multifunctional BAC transgenic mouse reporter. Dev. Biol. 271, 388–402 (2004).
53. Y. V. Wang, M. Weick, J. B. Demb, Spectral and temporal sensitivity of cone-mediated responses in mouse retinal ganglion cells. J. Neurosci. 31, 7670–7681 (2011).
54. D. M. Berson, F. A. Dunn, M. Takao, Phototransduction by retinal ganglion cells that set the circadian clock. Science 295, 1070–1073 (2002).
55. S. Hattar, H. W. Liao, M. Takao, D. M. Berson, K. W. Yau, Melanopsin-containing retinal ganglion cells: Architecture, projections, and intrinsic photosensitivity. Science 295, 1065–1070 (2002).
56. M. T. H. Do, K. W. Yau, Intrinsically photosensitive retinal ganglion cells. Physiol. Rev. 90, 1547–1581 (2010).
57. M. T. H. Do, Melanopsin and the intrinsically photosensitive retinal ganglion cells: Biophysics to behavior. Neuron 104, 205–226 (2019).
58. Q. Shi, P. Gupta, A. K. Boukhvalova, J. H. Singer, D. A. Butts, Functional characterization of retinal ganglion cells using tailored nonlinear modeling. Sci. Rep. 9, 8713 (2019).
59. J. W. Triplett, C. Pfeiffenberger, J. Yamada, B. K. Stafford, N. T. Sweeney, A. M. Litke, A. Sher, A. A. Koulakov, D. A. Feldheim, Competition is a driving force in topographic mapping. Proc. Natl. Acad. Sci. U.S.A. 108, 19060–19065 (2011).
60. J. L. Bedont, T. A. Le Gates, E. A. Slat, M. S. Byerly, H. Wang, J. Hu, A. C. Rupp, J. Qian, G. W. Wong, E. D. Herzog, S. Hattar, S. Blackshaw, Lhx1 controls terminal differentiation and circadian function of the suprachiasmatic nucleus. Cell Rep. 7, 609–622 (2014).
61. H. Kondo, I. Matsushita, T. Tahira, E. Uchio, S. Kusaka, Mutations in ATOH7 gene in patients with nonsyndromic congenital retinal nonattachment and familial exudative vitreoretinopathy. Ophthalmic Genet. 37, 462–464 (2016).
62. Q. L. Giudice, M. Leleu, G. L. Manno, P. J. Fabre, Single-cell transcriptional logic of cell-fate specification and axon guidance in early-born retinal neurons. Development 146, dev178103 (2019).
63. R. B. Hufnagel, T. T. Le, A. L. Riesenberg, N. L. Brown, Neurog2 controls the leading edge of neurogenesis in the mammalian retina. Dev. Biol. 340, 490–503 (2010).
64. H. Zhou, T. Yoshioka, J. Nathans, Retina-derived POU-domain factor-1: A complex POU-domain gene implicated in the development of retinal ganglion and amacrine cells. J. Neurosci. 16, 2261–2274 (1996).
65. S. W. Choy, C. W. Cheng, S. T. Lee, V. W. T. Li, M. N. Y. Hui, C. C. Hui, D. Liu, S. H. Cheng, A cascade of irx1a and irx2a controls shh expression during retinogenesis. Dev. Dyn. 239, 3204–3214 (2010).
66. P. Ekström, K. Johansson, Differentiation of ganglion cells and amacrine cells in the rat retina: Correlation with expression of HuC/D and GAP-43 proteins. Dev. Brain Res. 145, 1–8 (2003).
67. K. Kruger, A. S. Tam, C. Lu, D. W. Sretavan, Retinal ganglion cell axon progression from the optic chiasm to initiate optic tract development requires cell autonomous function of GAP-43. J. Neurosci. 18, 5692–5705 (1998).
68. P. Panza, A. A. Stko, H. M. Maischein, I. Koch, M. Flötenmeyer, G. J. Wright, K. Mandai, C. A. Mason, C. Söllner, The LRR-receptor Islr2 is required for retinal axon routing at the vertebrate optic chiasm. Neural Dev. 10, 23 (2015).
69. J. B. Miesfeld, M. E. Moon, A. N. Riesenberg, A. N. Contreras, R. A. Kovall, N. L. Brown, Rbpj direct regulation of Atoh7 transcription in the embryonic mouse retina. Sci. Rep. 8, 10195 (2018).
70. K. B. Moore, M. A. Logan, I. Aldiri, J. M. Roberts, M. Steele, M. L. Vetter, C8orf46 homolog encodes a novel protein Vexin that is required for neurogenesis in Xenopus laevis. Dev. Biol. 437, 27–40 (2018).

Downloaded from http://advances.sciencemag.org/ on April 8, 2021

learning across cellular measurements, platforms, tissues, and species. Cell Syst. 8, 395–411.e8 (2019).
75. C. Guo, K. S. Cho, Y. Li, K. Tchedre, C. Antolik, J. Ma, J. Chew, T. P. Utheim, X. A. Huang, H. Yu, M. T. A. Malik, N. Anzak, D. F. Chen, IGFBPL1 regulates axon growth through IGF 1 mediated signaling cascades. Sci. Rep. 8, 2054 (2018).
76. F. Zhang, C. Lu, C. Severin, D. W. Sretavan, GAP 43 mediates retinal axon interaction with lateral diencephalon cells during optic tract formation. Development 127, 969–980 (2000).
77. I. Soto, E. Oglesby, B. P. Buckingham, J. L. Son, E. D. O. Roberson, M. R. Steele, D. M. Inman, M. L. Vetter, P. J. Horner, N. Marsh Armstrong, Retinal ganglion cells downregulate gene expression and lose their axons within the optic nerve head in a mouse glaucoma model. J. Neurosci. 28, 548–561 (2008).
78. N. M. Tran, K. Shekhar, I. E. Whitney, A. Jacobi, I. Benhar, G. Hong, W. Yan, X. Adiconis, M. E. Arnold, J. M. Lee, J. Z. Levin, D. Lin, C. Wang, C. M. Lieber, A. Regev, Z. He, J. R. Sanes, Single cell profiles of retinal ganglion cells differing in resilience to injury reveal neuroprotective genes. Neuron 104, 1039–1055.e12 (2019).
79. B. A. Rheaume, A. Jereen, M. Bolisetty, M. S. Sajid, Y. Yang, K. Renna, L. Sun, P. Robson, E. F. Trakhtenberg, Single cell transcriptome profiling of retinal ganglion cells identifies cellular subtypes. Nat. Commun. 9, 2759 (2018).
80. P. J. Skene, S. Henikoff, An efficient targeted nuclease strategy for high resolution mapping of DNA binding sites. eLife 6, e21856 (2017).
81. Y. Zhang, T. Liu, C. A. Meyer, J. Eeckhoute, D. S. Johnson, B. E. Bernstein, C. Nusbaum, R. M. Myers, M. Brown, W. Li, X. S. Liu, Model based analysis of ChIP Seq (MACS). Genome Biol. 9, R137 (2008).
82. I. Aldiri, B. Xu, L. Wang, X. Chen, D. Hiler, L. Griffiths, M. Valentine, A. Shirinifard, S. Thiagarajan, A. Sablauer, M. E. Barabas, J. Zhang, D. Johnson, S. Frase, X. Zhou, J. Easton, J. Zhang, E. R. Mardis, R. K. Wilson, J. R. Downing, M. A. Dyer; St. Jude Children's Research Hospital – Washington University Pediatric Cancer Genome Project, The dynamic epigenetic landscape of the retina during development, reprogramming, and tumorigenesis. Neuron 94, 550–568.e10 (2017).
83. S. Heinz, C. Benner, N. Spann, E. Bertolino, Y. C. Lin, P. Laslo, J. X. Cheng, C. Murre, H. Singh, C. K. Glass, Simple combinations of lineage determining transcription factors prime cis regulatory elements required for macrophage and B cell identities. Mol. Cell 38, 576–589 (2010).
84. G. Yu, L. G. Wang, Q. Y. He, ChIPseeker: An R/Bioconductor package for ChIP peak annotation, comparison and visualization. Bioinformatics 31, 2382–2383 (2015).
85. O. Cordero Llana, F. Rinaldi, P. A. Brennan, D. Wynick, M. A. Caldwell, Galanin promotes neuronal differentiation from neural progenitor cells in vitro and contributes to the generation of new olfactory neurons in the adult mouse brain. Exp. Neurol. 256, 93–104 (2014).
86. F. E. Holmes, S. Mahoney, V. R. King, A. Bacon, N. C. H. Kerr, V. Pachnis, R. Curtis, J. V. Priestley, D. Wynick, Targeted disruption of the galanin gene reduces the number of sensory neurons and their regenerative capacity. Proc. Natl. Acad. Sci. U.S.A. 97, 11563–11568 (2000).
87. N. E. Baker, N. L. Brown, All in the family: Proneural bHLH genes and neuronal diversity. Development 145, dev159426 (2018).
88. A. I. Valenciano, P. Boya, E. J. de la Rosa, Early neural cell death: Numbers and cues from the developing neuroretina. Int. J. Dev. Biol. 53, 1515–1528 (2009).
89. J. M. Frade, P. Bovolenta, J. R. Martínez Morales, A. Arribas, J. A. Barbas, A. Rodríguez Tébar, Control of early cell death by BDNF in the chick retina. Development 124, 3313–3320 (1997).
90. L. Rodríguez Gallardo, M. del Carmen Lineros Domínguez, J. Francisco Morcillo, G. Martín Partido, Macrophages during retina and optic nerve development in the mouse embryo: Relationship to cell death and optic fibres. Anat. Embryol. 210, 303–316 (2005).
91. R. C. Strom, R. W. Williams, Cell production and cell death in the generation of variation in neuron number. J. Neurosci. 18, 9948–9953 (1998).
92. M. H. Farah, S. S. Easter Jr., Cell birth and death in the mouse retinal ganglion cell layer. J. Comp. Neurol. 489, 120–134 (2005).
93. T. T. Le, E. Wroblewski, S. Patel, A. N. Riesenberg, N. L. Brown, Math5 is required for both early retinal neuron differentiation and cell cycle progression. Dev. Biol. 295, 764–778 (2006).
98. Y. Jiang, Q. Ding, X. Xie, R. T. Libby, V. Lefebvre, L. Gan, Transcription factors SOX4 and SOX11 function redundantly to regulate the development of mouse retinal ganglion cells. J. Biol. Chem. 288, 18429–18438 (2013).
99. D. Sapkota, H. Chintala, F. Wu, S. J. Fliesler, Z. Hu, X. Mu, Onecut1 and Onecut2 redundantly regulate early retinal cell fates during development. Proc. Natl. Acad. Sci. U.S.A. 111, E4086–E4095 (2014).
100. O. Takeuchi, J. Fisher, H. Suh, H. Harada, B. A. Malynn, S. J. Korsmeyer, Essential role of BAX, BAK in B cell homeostasis and prevention of autoimmune disease. Proc. Natl. Acad. Sci. U.S.A. 102, 11272–11277 (2005).
101. L. Madisen, T. A. Zwingman, S. M. Sunkin, S. W. Oh, H. A. Zariwala, H. Gu, L. L. Ng, R. D. Palmiter, M. J. Hawrylycz, A. R. Jones, E. S. Lein, H. Zeng, A robust and high throughput Cre reporting and characterization system for the whole mouse brain. Nat. Neurosci. 13, 133–140 (2010).
102. T. C. Badea, H. Cahill, J. Ecker, S. Hattar, J. Nathans, Distinct roles of transcription factors Brn3a and Brn3b in controlling the development, morphology, and function of retinal ganglion cells. Neuron 61, 852–864 (2009).
103. J. M. McFarland, Y. Cui, D. A. Butts, Inferring nonlinear neuronal computation based on physiologically plausible inputs. PLOS Comput. Biol. 9, e1003143 (2013).
104. T. D. Sherman, T. Gao, E. J. Fertig, CoGAPS 3: Bayesian non negative matrix factorization for single cell analysis with asynchronous updates and sparse data structures. bioRxiv, 699041 (2019).
105. L. Haghverdi, M. Büttner, F. A. Wolf, F. Buettner, F. J. Theis, Diffusion pseudotime robustly reconstructs lineage branching. Nat. Methods 13, 845–848 (2016).
106. K. Polański, M. D. Young, Z. Miao, K. B. Meyer, S. A. Teichmann, J. E. Park, BBKNN: Fast batch alignment of single cell transcriptomes. Bioinformatics 36, 964–965 (2019).
107. C. Trapnell, D. Cacchiarelli, J. Grimsby, P. Pokharel, S. Li, M. Morse, N. J. Lennon, K. J. Livak, T. S. Mikkelsen, J. L. Rinn, The dynamics and regulators of cell fate decisions are revealed by pseudotemporal ordering of single cells. Nat. Biotechnol. 32, 381–386 (2014).
108. X. Qiu, A. Hill, J. Packer, D. Lin, Y. A. Ma, C. Trapnell, Single cell mRNA quantification and differential analysis with Census. Nat. Methods 14, 309–315 (2017).
109. T. Shimogori, D. A. Lee, A. Miranda Angulo, Y. Yang, H. Wang, L. Jiang, A. C. Yoshida, A. Kataoka, H. Mashiko, M. Avetisyan, L. Qi, J. Qian, S. Blackshaw, A genomic atlas of mouse hypothalamic development. Nat. Neurosci. 13, 767–775 (2010).
110. B. Langmead, S. L. Salzberg, Fast gapped read alignment with Bowtie 2. Nat. Methods 9, 357–359 (2012).
111. M. P. Meers, T. D. Bryson, J. G. Henikoff, S. Henikoff, Improved CUT&RUN chromatin profiling tools. eLife 8, e46314 (2019).
112. H. Li, B. Handsaker, A. Wysoker, T. Fennell, J. Ruan, N. Homer, G. Marth, G. Abecasis, R. Durbin; 1000 Genome Project Data Processing Subgroup, The Sequence Alignment/Map format and SAMtools. Bioinformatics 25, 2078–2079 (2009).
113. A. R. Quinlan, I. M. Hall, BEDTools: A flexible suite of utilities for comparing genomic features. Bioinformatics 26, 841–842 (2010).
114. F. Ramírez, D. P. Ryan, B. Grüning, V. Bhardwaj, F. Kilpert, A. S. Richter, S. Heyne, F. Dündar, T. Manke, deepTools2: A next generation web server for deep sequencing data analysis. Nucleic Acids Res. 44, W160–W165 (2016).
115. R. Morris, Developments of a water maze procedure for studying spatial learning in the rat. J Neurosci Meth. 11, 47–60 (1984).
116. P. Mombaerts, F. Wang, C. Dulac, S. K. Chao, A. Nemes, M. Mendelsohn, J. Edmondson, R. Axel, Visualizing an olfactory sensory map. Cell 87, 675–686 (1996).

Acknowledgments: We thank X. Mu and F. Wu for providing Atoh7$^{tTA/tTA}$;B&I-EE mice, L. Gan for providing Atoh7^{Cre} mice, N. Brown for technical advice, H. Hao and Hopkins Transcriptomics and Deep Sequencing Core for assistance with scRNA Seq, and W. Yap for comments on the manuscript. Funding: This work was supported by NIH grants R01EY020560 (S.B.), R00EY27844 (B.S.C.), EY19497 (T.G.), GM076430 and EY027202 (S.H. and H.Z.), EY021372 (J.S.), and F32 EY022543 (T.S.); the intramural research fund at the National Institute of Mental Health (MH002964) (S.H.); an unrestricted grant to the Department of Ophthalmology and

Downloaded from http://advances.sciencemag.org/ on April 8, 2021

Data and materials availability: All data needed to evaluate the conclusions in the paper are present in the paper and/or the Supplementary Materials. scRNA-seq–processed [expression, gene (featureData), and cell (phenoData) matrices] and raw sequence information (.bam files) are available for direct download through GEO GSE148814. Atoh7 Cut&Run data are available through GEO GSE156756. The mouse developmental scRNA-seq (23) and ATAC-seq datasets were downloaded from GSE118614 and GSE102092, respectively. ATAC-seq samples were realigned to mm10, to conform to scRNA-seq and Cut&Run datasets using the same pipeline as described for Cut&Run samples. Additional data related to this paper may be requested from the authors.

Submitted 25 August 2020
Accepted 29 January 2021
Published 12 March 2021
10.1126/sciadv.abe4983

Citation: J. Brodie-Kommit, B. S. Clark, Q. Shi, F. Shiau, D. W. Kim, J. Langel, C. Sheely, P. A. Ruzycki, M. Fries, A. Javed, M. Cayouette, T. Schmidt, T. Badea, T. Glaser, H. Zhao, J. Singer, S. Blackshaw, S. Hattar, Atoh7-independent specification of retinal ganglion cell identity. Sci. Adv. 7, eabe4983 (2021).

Downloaded from http://advances.sciencemag.org/ on April 8, 2021

ScienceAdvances

Atoh7-independent specification of retinal ganglion cell identity

Justin Brodie-Kommit, Brian S. Clark, Qing Shi, Fion Shiau, Dong Won Kim, Jennifer Langel, Catherine Sheely, Philip A Ruzycki, Michel Fries, Awais Javed, Michel Cayouette, Tiffany Schmidt, Tudor Badea, Tom Glaser, Haiqing Zhao, Joshua Singer, Seth Blackshaw and Samer Hattar

Sci Adv **7** (11), eabe4983.
DOI: 10.1126/sciadv.abe4983

ARTICLE TOOLS http://advances.sciencemag.org/content/7/11/eabe4983

SUPPLEMENTARY MATERIALS http://advances.sciencemag.org/content/suppl/2021/03/08/7.11.eabe4983.DC1

REFERENCES This article cites 113 articles, 35 of which you can access for free
http://advances.sciencemag.org/content/7/11/eabe4983#BIBL

PERMISSIONS http://www.sciencemag.org/help/reprints-and-permissions

Downloaded from http://advances.sciencemag.org/ on April 8, 2021